

AERO: SOFTMAX-ONLY LLMs FOR EFFICIENT PRIVATE INFERENCE

Anonymous authors

Paper under double-blind review

ABSTRACT

The pervasiveness of proprietary language models has raised privacy concerns for users' sensitive data, emphasizing the need for private inference (PI), where inference is performed directly on encrypted inputs. However, current PI methods face prohibitively higher communication and latency overheads, primarily due to nonlinear operations. In this paper, we present a comprehensive analysis to understand the role of nonlinearities in transformer-based decoder-only language models. We introduce AERO, a four-step architectural optimization framework that refines the existing LLM architecture for efficient PI by systematically removing nonlinearities such as LayerNorm and GELU and reducing FLOPs counts. For the *first time*, we propose a Softmax-only architecture with significantly fewer FLOPs tailored for efficient PI. Furthermore, we devise a novel entropy regularization technique to improve the performance of Softmax-only models. AERO achieves up to $4.23 \times$ communication and $1.94 \times$ latency reduction. We validate the effectiveness of AERO by benchmarking it against the state-of-the-art.

1 INTRODUCTION

Motivation. The widespread adoption of proprietary models like ChatGPT Achiam et al. (2023) significantly raised the privacy concerns to protect the users' sensitive (prompt) data Staab et al. (2024); Miresghallah et al. (2024); Priyanshu et al. (2023); Lauren & Knight (2023), while also preventing the attacks aimed at extracting model weights Carlini et al. (2024); Jovanović et al. (2024).

This emphasizes the need for private inference (PI) where a user sends the encrypted queries to the service provider without revealing their actual inputs, and the inference is performed directly on encrypted inputs, assuring the privacy of input and protection of the model's weight.

Despite their promises, current PI methods remain impractical due to their prohibitive latency and communication overheads—generating a single output token with GPT-2 model (125M parameters) on 128 input tokens takes 8.2 minutes and requires 25.3 GBs communication (Figure 1), scaling to 30.7 minutes and 145.2 GBs for context size of 512 (Table 7). These overheads stem largely from the nonlinear operations, crucial for model performance, in a transformer-based large language model (LLM), such as GELU, LayerNorm, and Softmax Hou et al. (2023); Lu et al. (2025).

Challenges. Current PI solutions for transformer-based models (e.g., ViT, BERT) either *neglect* the cost of LayerNorm (Li et al., 2023a; Zeng et al., 2023; Zhang et al., 2023; Chen et al., 2023) or approximate nonlinear operations using polynomial functions Zimerman et al. (2024); Dhyani et al. (2024). Nonetheless, polynomial approximation methods have their limitations: their accuracy is highly sensitive to data-specific initial guesses Knott et al. (2021), and their effectiveness is confined to narrow input ranges Zimerman et al. (2024). Moreover, networks employing higher-degree polynomials for improved approximation precision are notoriously difficult to train and optimize.

Meanwhile, the nonlinearity reduction methods, used for improving plaintext speed, offer *very-limited* potential to improve the PI efficiency. For instance, (He et al., 2023; Noci et al., 2023; He & Hofmann, 2024) has explored architectural heuristics to design LayerNorm-free LLMs; however, their broader implications on the choices of activation function, a key bottleneck in PI, remains largely unexamined.

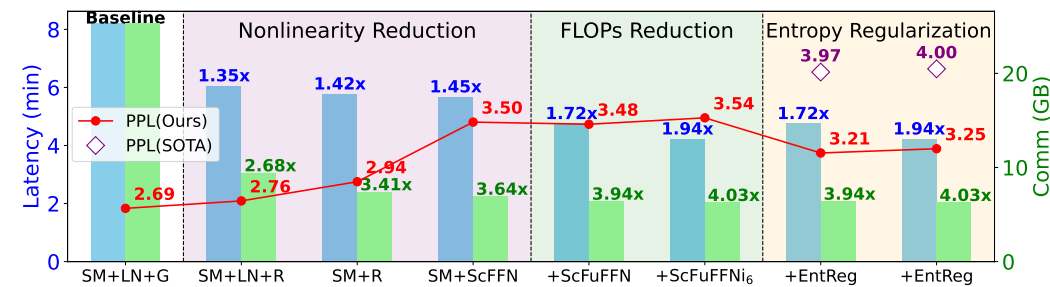


Figure 1: Latency and communication savings through nonlinearity and FLOPs reduction steps when AERO is applied on GPT-2, and trained from scratch on CodeParrot dataset. Further, we benchmark AERO against the SOTA He & Hofmann (2024) at iso-latency points. See Table 4 for a detail analysis.

Our techniques and insights. We conducted an in-depth analysis of the role of non-linearities in transformer-based LLMs. Our key findings are: (1) LayerNorm-free models exhibit a preference for ReLU over GELU in feed-forward network (FFN), making them more PI-friendly; and (2) training instability, as entropy collapse in deeper layers, in the Softmax-only model can be prevented by normalizing FFN weights, avoiding the nonlinear computations (unlike LayerNorm) at inference.

We observed a phenomenon we term *entropic overload*, where a disproportionately larger fraction of attention heads stuck at higher, close to their maximum, entropy values in LN-free with GELU, and Softmax-only models. We hypothesize that the entropic overload causes a lack of diversity and specialization in attention heads, squandering the representational capacity of attention heads. This leads to performance degradation, indicated by a higher perplexity.

To mitigate the entropic overload, we propose a novel entropy regularization technique that penalizes the extreme entropy values at training and avoids the deviation from well-behaved entropy distribution.

Results and implications. As shown in Figure 1, substituting GELU with ReLUs in the baseline GPT-2 model alone reduces the communication and latency overheads by $2.68\times$ and $1.35\times$, respectively. Eliminating LayerNorms further improves these savings to $3.41\times$ and $1.42\times$. Similar improvements are observed with the Pythia model (see Figure 15).

Since the FFN in the Softmax-only model is performing only the linear transformations, merging the linear layers into a single linear layer reduces the FFN FLOPs by $8\times$ and gains significant speedup *without increasing the perplexity* (see Figure 1). Furthermore, our analysis reveals that the linear transformations performed by early FFNs are crucial for training stability in the Softmax-only model, while deeper FFNs can be pruned. This provides additional opportunities for FLOPs reduction.

Contributions. Our key contributions are follows:

1. We thoroughly characterize the role of GELU and LayerNorm nonlinearities in transformer-based LLMs by examining their impact on the attention score distribution using Shannon’s entropy, offering insights for tailoring existing LLM architectures for efficient PI.
2. We introduced AERO, a four-stage optimization framework, and designed a Softmax-only model with fewer FLOPs, achieving up to $1.94\times$ speedup and $4.23\times$ communication reduction.
3. We introduce a novel entropy regularization technique to boost the performance of the Softmax-only model, which achieves **6% - 8%** improvement in perplexity.
4. We conducted extensive experiments across various context sizes (128, 256, 512) and model depths (12L and 18L) on a wide range of training tokens (1.2B to 4.8B) from the CodeParrot Face and Languini dataset Stanić et al. (2023) on GPT-2 and Pythia Biderman et al. (2023) models.

2 PRELIMINARIES

Notations. We denote the number of layers as L , number of heads as H , model dimensionality as d , head dimension as d_k (where $d_k = \frac{d}{H}$), and context length as T . Table 1 illustrates the abbreviations for architectural configurations with simplified nonlinearities in a transformer-based LLM.

An overview of transformer-based decoder-only architecture. A transformer-based LLM is constructed by sequentially stacking L transformer blocks, where each block is composed of two

108 sub-blocks: an attention mechanism and a feed-forward network (FFN), both having their own
 109 residual connections and normalization layers, positioned in the Pre-LN order to improves training
 110 stability (Xiong et al., 2020). Formally, transformer blocks take an input sequence $\mathbf{X}_{\text{in}} \in \mathbb{R}^{T \times d}$,
 111 consisting of T tokens of dimension d , and transform it into \mathbf{X}_{out} as follows:

$$\mathbf{X}_{\text{out}} = \hat{\mathbf{X}}_{\text{SA}} + \text{FFN}_{\text{GELU}}(\text{LayerNorm}_2(\hat{\mathbf{X}}_{\text{SA}})), \text{ where } \hat{\mathbf{X}}_{\text{SA}} = \mathbf{X}_{\text{in}} + \text{MHA}(\text{LayerNorm}_1(\mathbf{X}_{\text{in}})). \quad (1)$$

114 The Multi-Head Attention (MHA) sub-block enables input contextualization by sharing information
 115 between individual tokens. MHA employs the self-attention mechanism to compute the similarity
 116 score of each token with respect to all other tokens in the sequence. In particular, self-attention
 117 mechanism transform the input sequence \mathbf{X} into $\text{Attn}(\mathbf{X})$ as follows:

$$\text{Attn}(\mathbf{X}) = \left(\text{Softmax} \left(\frac{1}{\sqrt{d_k}} (\mathbf{X} \mathbf{W}^Q) (\mathbf{X} \mathbf{W}^K)^T + \mathbf{M} \right) \right) \mathbf{X} \mathbf{W}^V. \quad (2)$$

120 Here, each token generates query(Q), key(K), and value(V) vectors through the linear transformations
 121 \mathbf{W}^Q , \mathbf{W}^K , and $\mathbf{W}^V \in \mathbb{R}^{d \times d_h}$, respectively. Then, similarity scores are computed by taking the dot
 122 product of the Q and K vectors, scaled by the inverse square root of the K dimension, and passed
 123 through a softmax function to obtain the attention weights. These weights are then used to compute
 124 a weighted sum of the V vectors, producing the output for each token. For auto-regressive models
 125 (e.g., GPT), mask $\mathbf{M} \in \mathbb{R}^{T \times T}$, which has values in $\{0, -\infty\}$ with $\mathbf{M}_{i,j} = 0$ iff $i \geq j$, is deployed to
 126 prevent the tokens from obtaining information from future tokens.

127 The MHA sub-block employs a self-attention mechanism across all the heads, each with its own
 128 sets of Q , K , and V . This allows the attention heads to focus on different parts of the input
 129 sequence, capturing various aspects of the input data simultaneously. The outputs from all heads are
 130 concatenated and linearly transformed ($\mathbf{W}^O \in \mathbb{R}^{d \times d}$) to produce the final MHA output as follows:

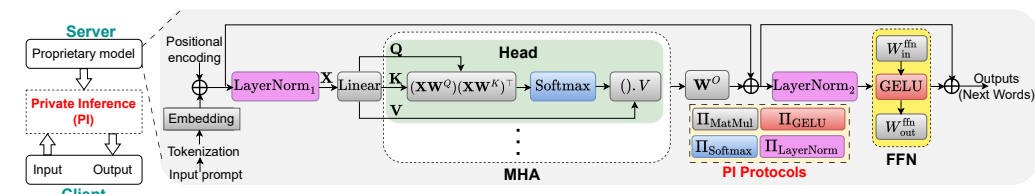
$$\text{MHA}(\mathbf{X}) = \text{Concat}(\text{Attn}_1(\mathbf{X}), \text{Attn}_2(\mathbf{X}), \text{Attn}_3(\mathbf{X}), \dots, \text{Attn}_H(\mathbf{X})) \mathbf{W}^O. \quad (3)$$

133 Following the MHA sub-block, the FFN sub-block transforms each token independently. The FFN
 134 sub-blocks have a single hidden layer whose dimension is a multiple of d (e.g., $4d$ in GPT (Radford
 135 et al., 2019) models). Specifically, the FFN sub-block first applies a linear transformation to the input
 136 \mathbf{X} using $\mathbf{W}_{\text{in}}^{\text{ffn}} \in \mathbb{R}^{d \times 4d}$, followed by a non-linear transformation using an activation function such as
 137 GELU. This is then followed by another linear transformation using $\mathbf{W}_{\text{out}}^{\text{ffn}} \in \mathbb{R}^{4d \times d}$, as follows:

$$\text{FFN}(\mathbf{X}) = (\text{GELU}(\mathbf{X} \mathbf{W}_{\text{in}}^{\text{ffn}})) \mathbf{W}_{\text{out}}^{\text{ffn}} \quad (4)$$

139 The combination of MHA and FFN sub-blocks, along with residual connections and normalization
 140 layers, allows transformer models to learn the contextual relationships between tokens effectively.

141 **Threat model for private inference.** We consider the standard two-party (2PC) client-server setting
 142 used in PPML, which provides security against semi-honest (honest-but-curious) adversaries bounded
 143 by probabilistic polynomial time Zhang et al. (2025); Lu et al. (2025); Pang et al. (2024); Hou et al.
 144 (2023). Both parties follow protocol specifications but may attempt to gain additional information
 145 from their outputs about the other party’s input. In this 2PC setting, the server holds the propriety
 146 GPT model (e.g., ChatGPT), and the client queries the model with a piece of text (prompt). The
 147 protocols ensure that the server does not know anything about the client’s input and the output of
 148 their queries, and the client does not know anything about the server’s model except its architecture.



156 Figure 2: An illustration of threat model and cryptographic protocols used for LLM private inference.

3 REMOVING NONLINEARITY IN TRANSFORMER-BASED LLMs

158 In this section, we investigate the role of non-linearities in the learning dynamics and internal
 159 representations of a transformer-based autoregressive decoder-only LLM. We design a controlled

experimental framework that systematically removes non-linear components from the architecture (see Table 1), and trains models from scratch.

Table 1: Architectural configurations of nonlinearities in LLMs, illustrating the combinations of Softmax (SM), LayerNorm (LN), GELU (G), and ReLU (R) functions (see Eq. 1, 2, 3 and 4).

Abbreviation	Architectural configuration
SM + LN + G	$\mathbf{X}_{\text{out}} = \text{FFN}_{\text{GELU}}(\text{LayerNorm}_2(\text{MHA}(\text{Attn}_{\text{Softmax}}(\text{LayerNorm}_1(\mathbf{X}_{\text{in}})))))$
SM + LN + R	$\mathbf{X}_{\text{out}} = \text{FFN}_{\text{ReLU}}(\text{LayerNorm}_2(\text{MHA}(\text{Attn}_{\text{Softmax}}(\text{LayerNorm}_1(\mathbf{X}_{\text{in}})))))$
SM + LN	$\mathbf{X}_{\text{out}} = \text{FFN}_{\text{Identity}}(\text{LayerNorm}_2(\text{MHA}(\text{Attn}_{\text{Softmax}}(\text{LayerNorm}_1(\mathbf{X}_{\text{in}})))))$
SM + G	$\mathbf{X}_{\text{out}} = \text{FFN}_{\text{GELU}}(\text{MHA}(\text{Attn}_{\text{Softmax}}(\mathbf{X}_{\text{in}})))$
SM + R	$\mathbf{X}_{\text{out}} = \text{FFN}_{\text{ReLU}}(\text{MHA}(\text{Attn}_{\text{Softmax}}(\mathbf{X}_{\text{in}})))$
SM	$\mathbf{X}_{\text{out}} = \text{FFN}_{\text{Identity}}(\text{MHA}(\text{Attn}_{\text{Softmax}}(\mathbf{X}_{\text{in}})))$

To analyze internal representations, we use Shannon’s entropy to examine the impacts of nonlinearities on the attention score distribution (see Appendix A.1 for its justification). We highlight key insights and findings, offering practical guidelines for tailoring LLM architectures for efficient PI.

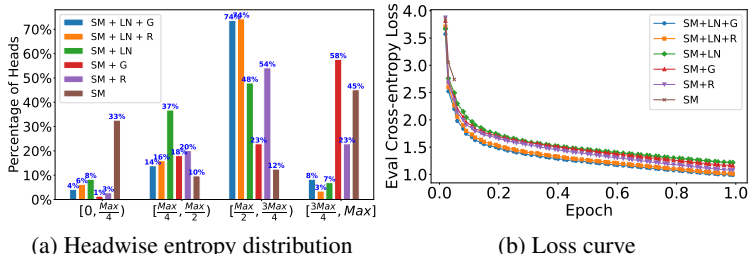


Figure 3: (a) The fraction of attention heads distributed across different entropy ranges, and (b) evaluation loss for GPT-2 (small) models with fewer nonlinearities, corresponding to Figure 3b. Δ is increase in PPL over baseline network.

Configurations	PPL	$+\Delta(\%)$
SM + LN + G	2.69	0.00
SM + LN + R	2.76	2.53
SM + LN	3.38	25.58
SM + G	3.20	18.92
SM + R	2.94	9.20
SM	NanNs	-

Table 2: Evaluation perplexity for GPT-2 (small) models with fewer nonlinearities, corresponding to Figure 3b. Δ is increase in PPL over baseline network.

Well-behaved entropy distribution We begin by analyzing the headwise entropy distribution of baseline architecture with GELU and ReLU in the FFN, i.e., configurations SM + LN + G and SM + LN + R respectively. We find that the majority of heads ($\approx 90\%$) possess entropy values between $\frac{\text{max}}{4}$ and $\frac{3\text{max}}{4}$, where max is maximum observed entropy value among all heads (see Figure 3a). This concentration in the mid-entropy range, while avoiding extremes, demonstrates a well-behaved distribution, providing a benchmark for assessing the impact of nonlinearities on model behavior.

Entropic overload We observed that in certain nonlinearity configurations, a disproportionately large fraction of the attention heads exhibit higher entropy values (between $\frac{3\text{max}}{4}$ and max). We term this phenomenon as entropic overload and hypothesize that this imbalance results in *under-utilization* of the network’s representational capacity, as too many heads engaged in exploration, hindering the model from effectively leveraging the diversity of attention heads.

To investigate further, we examined how entropy values evolve during training. Typically, all heads start with higher entropy values, indicating an initial exploration phase, and gradually adapt to balance exploration and exploitation in baseline networks (see Figure 12). However, in the absence of certain nonlinearities, this balance is disrupted, preventing attention heads from specializing and refining their focus on critical aspects of the input, thereby diminishing overall performance.

3.1 DESIRABLE ACTIVATION FUNCTION IN LAYERNORM-FREE LLMs

We first remove LayerNorm from the LLM architecture and study the desirable activation function in this design, as the absence of LayerNorm can destabilize activation statistics.

Observation 1: ReLU significantly outperforms GELU in LayerNorm-Free LLMs. While GELU is typically preferred over ReLU in conventional transformer-based models due to its smooth and differentiable properties that improve performance and optimization, our empirical findings indicate the *opposite trend* for LayerNorm-free models—using ReLU in the FFN exhibit better learning

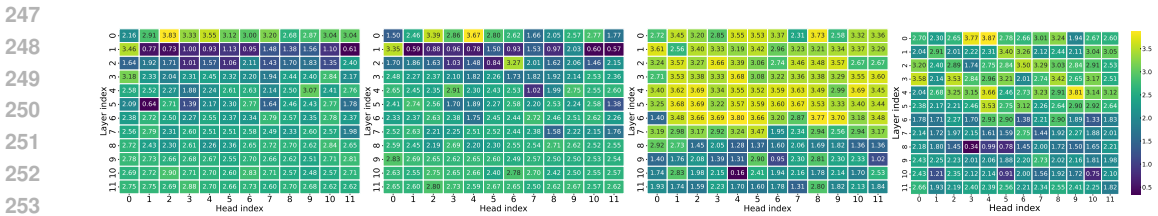
216 dynamics than their GELU counterpart. This leads to an **8.2%** improvement in perplexity for GPT-2
 217 (see Figure 3 and Table 2). A similar trend has been observed on the LN-free Pythia-70M model
 218 across various context lengths (see Table 8).

219 To further strengthen our findings,
 220 we conducted experiments with
 221 a learnable negative slope in the
 222 leaky ReLU activation function
 223 with two configurations: 1) layer-
 224 wise, where each layer has its in-
 225 dependent learnable slope, and 2)
 226 global, where a single learnable
 227 slope is shared across all layers.
 228 Results are shown in Figure 4. In-
 229 terestingly, in the layerwise set-
 230 ting, the early layers initially learn
 231 a positive slope while the deeper layers learn a negative slope. However, as training progresses, all
 232 layers converge to a near-zero slope. In the global setting, the slope first shifts to positive before
 233 converging to near zero. Refer to Figure 13 for their layerwise entropy dynamics.

234 This highlights the distinct learning dynamics of nonlinearity choices, and a natural preference for
 235 zero negative slope, similar to ReLU, in the FFN activation function of the LN-free model.

236 **Observation 2: Early layers in the LayerNorm-Free model with GELU in FFN experience**
 237 **entropic overload.** To understand the zero negative slope preference for the FFN activation function
 238 in LN-free architecture, we analyzed the headwise entropy values of LN-free models with GELU and
 239 ReLU, when trained from scratch, and compared them to their baseline counterparts. Our analysis
 240 revealed a significant divergence in the headwise entropy distributions of the LN-free GELU model
 241 (see Figure 5). While baseline models with GELU and ReLU exhibit a balanced entropy distribution,
 242 by avoiding the extreme values, the LN-free GELU model shows entropic overload in early layers.

243 Specifically, 58% of heads in the LN-free GELU model have entropy values between $\frac{3\max}{4}$ and \max ,
 244 compared to only 23% in the LN-free ReLU model (Figure 3a). More importantly, very few heads
 245 in the latter approach maximum entropy compared to the former (see yellow regions in Figure 5c),
 246 indicating more severe entropic overload in the LN-free model with GELU.



(a) Layerwise learnable slope (b) Global learnable slope

Figure 4: Learnable negative slope for leaky ReLU in the FFN of LN-free GPT-2. (a) Layerwise slopes and (b) global slope, both converge toward zero during training, indicating a preference for zero negative slope in LN-free architectures.

Figure 5: Entropy heatmaps of attention for baseline GPT-2 models with GELU and ReLU in the FFN (a and b), compared to their LayerNorm-free counterparts (c and d). In the absence of LayerNorm, using GELU in the FFN results in significantly higher entropic overload than using ReLU.

Figure 5: Entropy heatmaps of attention for baseline GPT-2 models with GELU and ReLU in the FFN (a and b), compared to their LayerNorm-free counterparts (c and d). In the absence of LayerNorm, using GELU in the FFN results in significantly higher entropic overload than using ReLU.

258 These observations align with the geometrical properties of ReLUs: they preserve more information
 259 about the structure of the raw input, encouraging neurons to specialize in different regions of the
 260 input space, leading to a higher intra-class *selectivity* and *specialization* (Alleman et al., 2024). Thus,
 261 the lack of LayerNorm makes the geometry and specialization effects of ReLU more beneficial.

262 3.2 APPROACHES TO PREVENT TRAINING COLLAPSE IN SOFTMAX-ONLY LLMs

265 Now, we eliminate the ReLU layer in FFN of LN-free design, resulting in a Softmax-only architecture
 266 where FFN is fully linear, and the softmax operation becomes the only source of nonlinearity in the
 267 model. We outline the key challenges in training this model and explore their potential solutions.

268 **Observation 3: The softmax-only model exhibits severe entropic overload in the early layers**
 269 **and entropy collapse in the deeper layers.** When we train the softmax-only model from scratch, the
 loss values quickly reach NaN and training collapses. Analyzing the layer-by-layer activation values

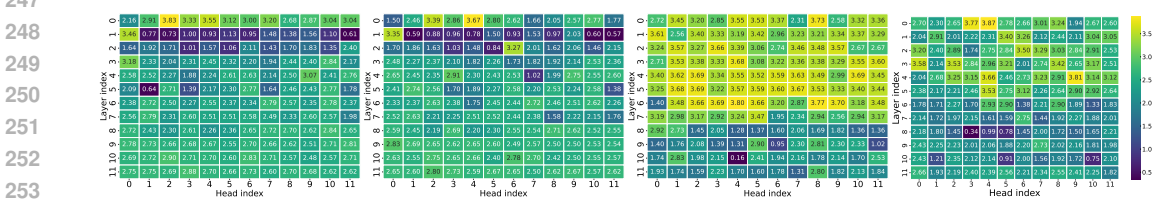


Figure 5: Entropy heatmaps of attention for baseline GPT-2 models with GELU and ReLU in the FFN (a and b), compared to their LayerNorm-free counterparts (c and d). In the absence of LayerNorm, using GELU in the FFN results in significantly higher entropic overload than using ReLU.

reveals that activations of the last few layers reach NaN very early in the training phase (Figure 6a). Further investigation into headwise entropy distribution shows that the early layers experience severe entropic overload (Figure 6b), as most of the heads in these layers are stuck at maximum entropy levels (the yellow regions). Conversely, the deeper layers suffer from entropy collapse, characterized by very low entropy values (the blue regions).

Quantitatively, 45% of total heads have entropy values in the range of $\frac{3\text{max}}{4}$ to max, with most close to the maximum value (Figure 3a), indicating severe entropic overload. Whereas, 33% of heads exhibit values in the entropy range of 0 to $\frac{\text{max}}{4}$, with most close to zero, indicating entropy collapse, a known indicator of training instability in transformer-based models (Zhai et al., 2023; He et al., 2024).

Observation 4: Normalizing the weights in FFN linear layers or appropriately scaling FFN outputs effectively prevents training collapse in softmax-only models. To prevent training collapse while maintaining PI efficiency, we shift from activation normalization to weight normalization techniques that avoid nonlinear computations at inference. While LayerNorm requires expensive inverse-square-root operations during inference, weight normalization (Salimans & Kingma, 2016) and spectral normalization (Miyato et al., 2018) offer static alternatives. These normalization methods, normalize the weights rather than the activations, incurring no additional cost at inference.

Weight normalization reparameterizes the weight vectors as $\mathbf{W}_{\text{normalized}} = \frac{\mathbf{V}}{\|\mathbf{V}\|_2}g$, where \mathbf{V} is reparameterized weight vector, $\|\mathbf{V}\|_2$ is Euclidean norm and g is a learnable scaling factor. Whereas, spectral normalization normalizes the weight matrix \mathbf{W} by its largest singular value $\sigma(\mathbf{W})$, yielding $\mathbf{W}_{\text{normalized}} = \frac{\mathbf{W}}{\sigma(\mathbf{W})}$. The former uses the Euclidean norm to control the magnitude of the weights during the training while the latter uses the largest singular value to constrain the Lipschitz constant of the linear layers. We employed these normalizations in the FFN of the softmax-only model which transform $\text{FFN}^{\text{SM}}(\mathbf{X}) = (\mathbf{X}\mathbf{W}_{\text{in}}^{\text{ffn}})\mathbf{W}_{\text{out}}^{\text{ffn}}$ as follows:

$$\text{FFN}_{\text{WNorm}}^{\text{SM}}(\mathbf{X}) = \left(\mathbf{X} \frac{\mathbf{V}_{\text{in}}^{\text{ffn}}}{\|\mathbf{V}_{\text{in}}\|_2} g_{\text{in}} \right) \frac{\mathbf{V}_{\text{out}}^{\text{ffn}}}{\|\mathbf{V}_{\text{out}}\|_2} g_{\text{out}} \quad \text{and} \quad \text{FFN}_{\text{SNorm}}^{\text{SM}}(\mathbf{X}) = \left(\mathbf{X} \frac{\mathbf{W}_{\text{in}}^{\text{ffn}}}{\sigma(\mathbf{W}_{\text{in}}^{\text{ffn}})} \right) \frac{\mathbf{W}_{\text{out}}^{\text{ffn}}}{\sigma(\mathbf{W}_{\text{out}}^{\text{ffn}})} \quad (5)$$

Furthermore, we employ a simpler technique to scale the outputs of the FFN sub-block by having learnable scaling factors for the FFN output and their residual output as follows (see Eq. 1):

$$\mathbf{X}_{\text{out}} = \beta \hat{\mathbf{X}}_{\text{SA}} + \frac{1}{\alpha} (\text{FFN}^{\text{SM}}(\mathbf{X}_{\text{SA}})) \quad \text{where} \quad \alpha, \beta \in \mathbb{R}^L \quad (6)$$

Figure 7 demonstrates the effectiveness of these normalization techniques in stabilizing the training of softmax-only GPT-2 models by preventing entropy collapse in deeper layers. When comparing performance, we find that weight and spectral normalization led to similar performance while the learnable scaling method outperformed them with a lower perplexity (Table 3).

Note that the efficacy of weight or spectral normalization hinges on selecting the appropriate linear layers, as applying them to the linear layers in attention sub-block *diminishes* overall performance (see Table 9). Refer to Appendix D.1 to understand the effectiveness of the learnable scaling method.

4 AERO

We propose an AERO framework that tailors the existing LLM architecture by removing nonlinearity and reducing FLOPs count through targeted architectural refinements. Further, we introduce our entropy regularization technique to improve the performance of the Softmax-only model.

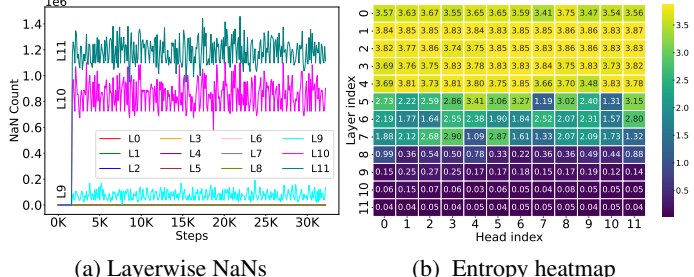


Figure 6: Training collapses in softmax-only GPT-2 model.
 (a) Layerwise NaNs (b) Entropy heatmap

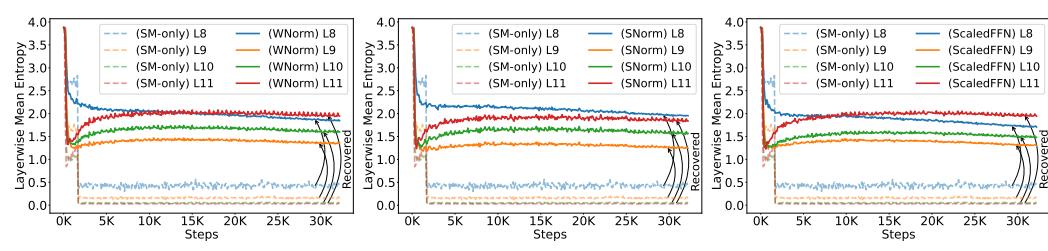


Figure 7: Mitigating entropy collapse in the deeper layers of a softmax-only GPT-2 model by employing weight or spectral normalization in FFN, or by appropriately scaling FFN block outputs.

4.1 DESIGNING SOFTMAX-ONLY ARCHITECTURE

To eliminate nonlinearities in existing LLM architectures, we first remove normalization layers, creating an LN-free design. Our approach extends previous work on LN-free design (He et al., 2023; Noci et al., 2023; He & Hofmann, 2024) by also carefully selecting FFN activation functions, opting for ReLU due to its superior PI efficiency and ability to mitigate entropic overload in LN-free models.

We then remove ReLU, leading to a full normalization and activation-free, or Softmax-only, architecture. Training this architecture, however, poses challenges, such as entropy collapse in deeper layers. To address this, we introduce learnable scaling factors, α and β , in the FFN sub-block, which stabilize training more effectively than weight or spectral normalization.

4.2 FLOPs REDUCTION IN SOFTMAX-ONLY ARCHITECTURE

To develop an effective FLOPs reduction strategy, we begin by analyzing the distribution of FLOPs between the attention and FFN sub-blocks across varying context lengths.

FFN FLOPs dominates in shorter context length regimes ($T < \frac{8}{3}d$). While prior work on LN-free architectures (He & Hofmann, 2024) has emphasized reducing attention FLOPs, we find that the network’s FLOPs are dominated by FFN FLOPs during inference with shorter context lengths (when $T < \frac{8}{3}d$, Eq. 13). For instance, when $T \leq 1K$, FFN FLOPs constitute 60%-65% of the total FLOPs in models like GPT-2 (Figure 20) and Pythia (Figure 21) variants.

Given that current research on 2PC PI primarily focuses on smaller context lengths (Zhang et al., 2025; Lu et al., 2025; Zimerman et al., 2024; Pang et al., 2024; Gupta et al., 2024; Hou et al., 2023), we strategically target reducing FFN FLOPs. First, we merge the two linear layers in FFN of Softmax-only architecture— $\mathbf{W}_{\text{in}}^{\text{ffn}} \in \mathbb{R}^{d \times 4d}$ and $\mathbf{W}_{\text{out}}^{\text{ffn}} \in \mathbb{R}^{4d \times d}$ —into a single linear layer, $\mathbf{W}^{\text{ffn}} \in \mathbb{R}^{d \times d}$, as they effectively perform linear transformation in the absence of intervening nonlinearity. This reduces FFN FLOPs by a $8\times$ without any performance degradation, which is not achievable in polynomial transformers, where GELU is approximated by polynomials (Zimerman et al., 2024; Li et al., 2023a).

To reduce FFN FLOPs even further, we ask the following questions: What functional role do FFNs serve when they are *purely linear*? Do all FFNs contribute *equally*, or can some of them be pruned?

Early FFNs in Softmax-only architecture are critical, while deeper ones can be pruned. We observe that early FFNs, despite being purely linear, are crucial for *training stability*, as their removal leads to entropy collapses (Fig. 16 and Fig. 17). Deeper FFNs, however, exhibit redundancy, allowing additional FLOPs reduction without degrading performance. This observation resonates with findings on the significance of early-to-mid (conventional non-linear) FFNs (Nanda et al., 2023; Sharma et al., 2024; Jin et al., 2024; Hu et al., 2024a; Stolfo et al., 2023; Wang et al., 2023; Haviv et al., 2023; Meng et al., 2022) and the redundant FFN computations (Kobayashi et al., 2024; Pires et al., 2023).

This enables an additional opportunity to reduce FFN FLOPs by selectively removing deeper FFNs. In Softmax-only GPT-2-small architecture, we successfully remove up to six deeper FFNs, achieving an additional $6\times$ FLOPs reduction in FFN. We refer to this simplified model as SM + ScFuFFN $_x$, where x represents the number of deeper FFNs that are replaced with identity functions, while the remaining FFNs have one (fused) linear layer. When $x=0$, we represent the model as SM + ScFuFFN.

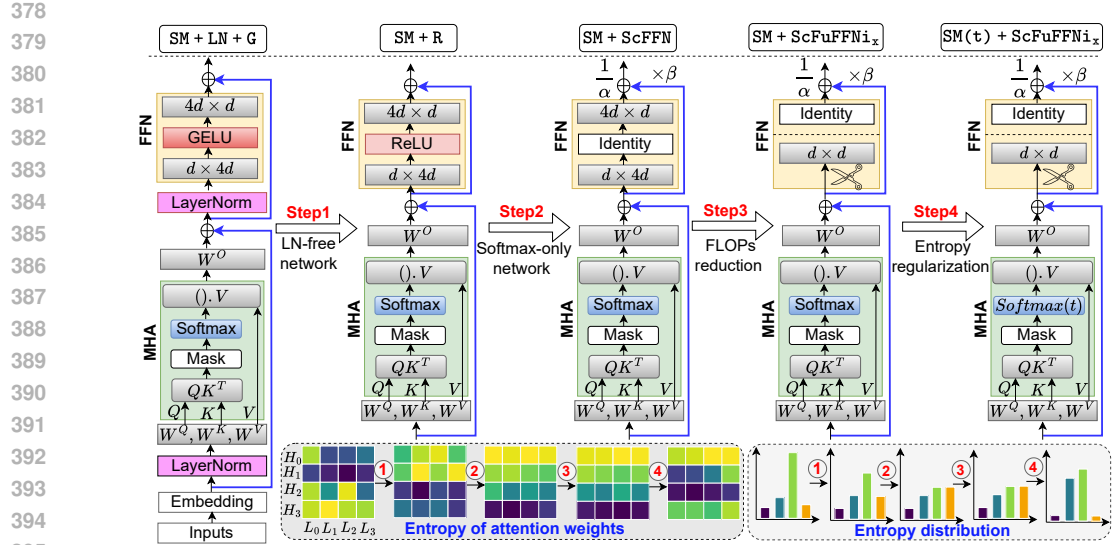


Figure 8: Overview of the proposed AERO method for reducing nonlinearities and FLOPs in transformer-based LLMs for efficient PI. The bottom of the figure shows the evolution of entropy in the attention mechanism and its distribution across attention heads.

4.3 ENTROPY REGULARIZATION

Challenges in designing entropy regularization schemes to prevent entropic overload. Previous entropy regularization approaches have primarily aimed at penalizing low-entropy predictions (Setlur et al., 2022; Pereyra et al., 2017), based on the principle of maximum entropy (Jaynes, 1982). Recently, (He et al., 2024) introduced entropy regularization to prevent entropy collapses, by addressing extremely low entropy values, in LLMs.

However, our goal is to regularize higher entropy values, which presents two-fold challenges: (1) *Head specialization*: Since each attention head captures different aspects of the input, the regularization strength needs to be adjusted for each head individually. (2) *Preventing over-regularization*: Some heads naturally exhibit higher entropy even in well-behaved entropy distributions, thus, penalizing all high-entropy values without distinction could be harmful, requiring a more flexible approach.

Key design principles for entropy regularization. Followings are the key design principles for our entropy regularization scheme (see Algorithm 1), addressing the aforementioned challenges:

- *Balanced entropy distribution with parameterized attention matrix*: Inspired by Miller et al. (1996), which used temperature parameter as a Lagrangian multiplier to control the entropy of a stochastic system, we parameterized the attention matrix by a learnable temperature $t \in \mathbb{R}^{H \times T}$ for each softmax operation, allowing the model to adjust the sharpness of the attention scores (see Appendix A.3). A higher temperature value ($t > 1$) diffuses the attention scores and increases the entropy, while a lower temperature value ($t < 1$) sharpens the attention scores and reduces the entropy.
- *Dynamic thresholds with head-specific adaptation*: To adapt the regularization strength based on the characteristics of each attention head (Voita et al., 2019), we use headwise learnable threshold parameter $\text{reg_threshold_weights} \in \mathbb{R}^H$. Consequently, the threshold for each head is computed as a learnable fraction of the maximum value of entropy ($\text{reg_threshold_weights} \times E_{\max}$), providing the fine-grained control (see Algorithm 1, line #11).
- *Tolerance margin to prevent over-regularization*: To prevent over-regularization, we allow small deviations from the respective thresholds. Thus, a penalty is imposed only if the deviation from the threshold exceeds the tolerance margin, which is set as a fraction of E_{\max} using the hyper-parameter γ (see Algorithm1, line #3).

$$\text{penalty}^{(l,h)} = \begin{cases} \left(\text{deviation}^{(l,h)}\right)^2 & \text{if } |\text{deviation}^{(l,h)}| > \gamma E_{\max} \\ 0 & \text{otherwise} \end{cases}$$

The deviation from threshold is computed as $\text{deviation}^{(l,h)} = E^{(l,h)}(t) - \theta^{(l,h)}E_{\max}$, where $\theta^{(l,h)}$ is $\text{reg_threshold_weights}$. The hyper-parameter γ ensures that the model is not excessively

- 432 penalized for minor deviations from the desired entropy threshold, which could impede its capacity
 433 to learn effectively. This careful calibration between stringent regularization and desired flexibility
 434 improves the model’s robustness while maintaining its adaptability to various input distributions.
 435 • *Maximum entropy reference:* We set $E_{\max} = \log(T)$ as a reference point for computing thresholds
 436 and tolerance margins to ensure consistency across different layers and heads for regularization.
 437 Additionally, it enhances interpretability by providing a quantifiable reference for measuring
 438 deviations in entropy, making the regularization process more understandable.

440 4.4 PUTTING IT ALL TOGETHER

442 We developed the AERO framework (Figure 8) to systematically eliminate non-linearities and reduce
 443 FFN FLOPs from the existing transformer-based LLMs. Given an input baseline LLM, the first two
 444 steps, Step1 and Step2, attempt to address the overheads associated with non-linear operations in
 445 PI, resulting in a softmax-only architecture. The next step, Step3, aims at reducing FFN FLOPs by
 446 fusing the adjacent linear layers, and then selectively pruning deeper FFNs by replacing them with
 447 identity functions, resulting in a substantial reduction in FLOPs without destabilizing the model.

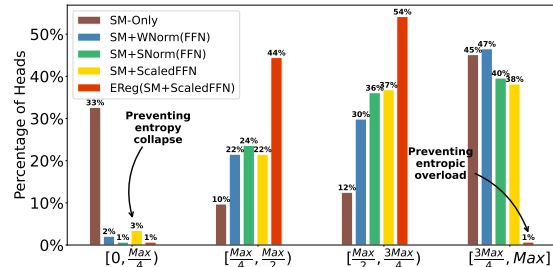
448 Further, to mitigate the entropic overload, and improve the utilization of attention heads, Step4
 449 introduces entropy regularization, keeping the balanced attention distributions by penalizing extreme
 450 entropy values. This step plays a crucial role in boosting the performance of the softmax-only model.

452 5 RESULTS

455 We conducted experiments with GPT-2 (12 and 18 layers) and Pythia-70M models on the CodeParrot
 456 and Languini book datasets, which are standard benchmarks for LLMs (He & Hofmann, 2024; He
 457 et al., 2024). For experimental setup and cryptographic protocols details, refer to Appendix C.

458 Entropy regularization prevents entropic overload in Softmax-only models

459 While both weight and spectral normalization
 460 and scaling methods effectively prevent
 461 entropy collapse in the deeper layers and sta-
 462 bilize the training of Softmax-only models,
 463 they fail to address the issue of entropic over-
 464 load, (see Figure 9). In contrast, the entropy
 465 regularization scheme penalizes the model to
 466 avoid extreme entropy values during training,
 467 resulting in a more balanced distribution. As a
 468 result, it complements the training stabilizing
 469 methods by further mitigating entropic over-
 470 load in the early layers (see Figure 14), im-
 471 proving the utilization of attention heads and
 472 leading to improved performance, as demon-
 473 strated by lower perplexity.



474 Figure 9: While normalizing weights or scaling out-
 475 puts in the FFN of Softmax-only (GPT-2) model pre-
 476 vents entropy collapse, our proposed entropy regular-
 477 ization effectively mitigates entropic overload.

478 **Comparison of AERO vs SOTA.** We apply AERO to GPT-2, with results for each step shown
 479 in Figure 1 and a detailed analysis in Table 4. Our approach achieves up to a $4\times$ reduction in
 480 communication overhead and a $1.94\times$ speedup in end-to-end PI latency.

481 We also applied AERO optimizations to the LayerNorm-free design proposed in (He & Hofmann,
 482 2024), referred to as SOTA, as they preserve model performance in their normalization-free archi-
 483 tecture. While SOTA saves additional attention FLOPs, by introducing one extra LayerNorm layer,
 484 compared to AERO, it offers a slight speedup at the cost of significantly worse model performance, as
 485 indicated by higher perplexity. Similar observations hold for the Pythia-70M model (see Figure 15).

486 In terms of scalability, AERO efficiently scales to deeper models (see Table 6) and larger context
 487 lengths (see Table 5 and Table 7), whereas SOTA often suffers from training instability under these
 488 conditions. Since the contribution of MHA to the model’s pre-training performance becomes more
 489 critical in the absence of FFN operations (Lu et al., 2024), we suspect that the aggressive optimization
 490 of attention FLOPs in SOTA, unlike AERO, results in inferior performance and training instability.

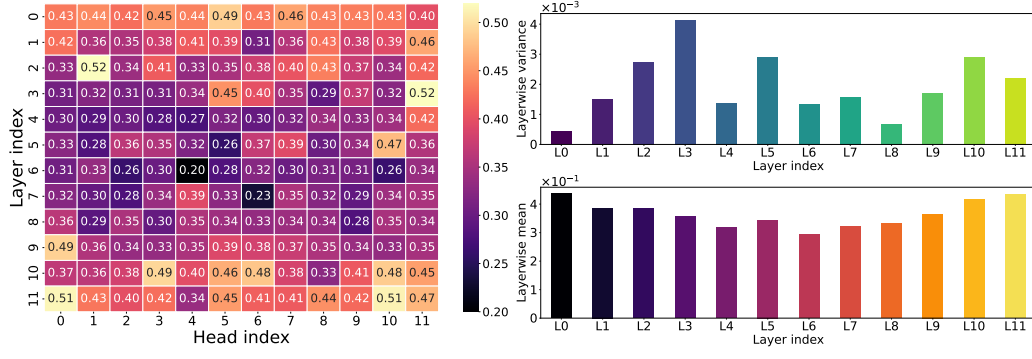
486
487
488
489
490
491
492
493
494
495
496
497
498
499
500
501
502
503
504
505
506
507
508
509
510
511
512
513
514
515
516
517
518
519
520
521
522
523
524
525
526
527
528
529
530
531
532
533
534
535
536
537
538
539

Table 4: Results, and comparison against SOTA (He & Hofmann, 2024), when GPT-2 ($L=12$, $H=12$, $d=768$) model is trained from scratch on CodeParrot (Face) dataset with context length 128.

	Network Arch.	PPL	#Nonlinear Ops	#FLOPs		Comm. (GB)	Lat. (min.)	Savings	
				FFN	Attn.			Comm.	Lat.
Baseline	SM + LN + G	2.69	SM:144 × $\mathbb{R}^{128 \times 128}$ LN:24 × $\mathbb{R}^{128 \times 768}$ G:12 × $\mathbb{R}^{128 \times 3072}$	14.5B	7.7B	25.32	8.21	1×	1×
	SM + LN + R	2.76	SM:144 × $\mathbb{R}^{128 \times 128}$ LN:24 × $\mathbb{R}^{128 \times 768}$ R:12 × $\mathbb{R}^{128 \times 3072}$	14.5B	7.7B	9.44	6.06	2.68×	1.35×
SOTA	SM + ScFFN	4.00	SM:144 × $\mathbb{R}^{128 \times 128}$ LN: 1 × $\mathbb{R}^{128 \times 768}$	14.5B	3.9B	6.83	5.31	3.71×	1.55×
	SM + ScFuFFN	3.97	SM:144 × $\mathbb{R}^{128 \times 128}$ LN: 1 × $\mathbb{R}^{128 \times 768}$	1.8B	3.9B	6.31	4.50	4.00×	1.82×
	SM + ScFuFFNi ₁	4.00	SM:144 × $\mathbb{R}^{128 \times 128}$ LN: 1 × $\mathbb{R}^{128 \times 768}$	1.2B	3.9B	6.30	4.44	4.00×	1.85×
AERO	SM + ScFFN	3.50	SM:144 × $\mathbb{R}^{128 \times 128}$	14.5B	7.7B	6.95	5.68	3.64×	1.45×
	SM + ScFuFFN	3.48	SM:144 × $\mathbb{R}^{128 \times 128}$	1.8B	7.7B	6.43	4.76	3.94×	1.72×
	SM + ScFuFFNi ₆	3.54	SM:144 × $\mathbb{R}^{128 \times 128}$	0.9B	7.7B	6.29	4.23	4.00×	1.94×
	EReg(SM(t) + ScFuFFN)	3.21	SM:144 × $\mathbb{R}^{128 \times 128}$	1.8B	7.7B	6.43	4.76	3.94×	1.72×
	EReg(SM(t) + ScFuFFNi ₆)	3.25	SM:144 × $\mathbb{R}^{128 \times 128}$	0.9B	7.7B	6.29	4.23	4.00×	1.94×

506
507
508
509
510
511
512
513
514
515
516
517
518
519
520
521
522
523
524
525
526
527
528
529
530
531
532
533
534
535
536
537
538
539

Significance of learnable thresholds in entropy regularization Figure 10 depicts the learnable threshold parameters (`reg_threshold_weights`) applied in the entropy regularization scheme after the model has been fully trained from scratch. They exhibit significant variability, both across layers and within individual heads of each layers, which reflects the model’s ability to dynamically adjust the regularization strength in response to the specific roles of different attention heads. Such flexibility is essential for tailoring the regularization process to the distinct requirements of each head.



(a) Values of learned threshold weights (b) Layerwise mean and variance of threshold weights

530
531
532
533
534
535
536
537
538
539
540
541
542
543
544
545
546
547
548
549
550
551
552
553
554
555
556
557
558
559
560
561
562
563
564
565
566
567
568
569
570
571
572
573
574
575
576
577
578
579
580
581
582
583
584
585
586
587
588
589
590
591
592
593
594
595
596
597
598
599
600
601
602
603
604
605
606
607
608
609
610
611
612
613
614
615
616
617
618
619
620
621
622
623
624
625
626
627
628
629
630
631
632
633
634
635
636
637
638
639
640
641
642
643
644
645
646
647
648
649
650
651
652
653
654
655
656
657
658
659
660
661
662
663
664
665
666
667
668
669
670
671
672
673
674
675
676
677
678
679
680
681
682
683
684
685
686
687
688
689
690
691
692
693
694
695
696
697
698
699
700
701
702
703
704
705
706
707
708
709
710
711
712
713
714
715
716
717
718
719
720
721
722
723
724
725
726
727
728
729
730
731
732
733
734
735
736
737
738
739
740
741
742
743
744
745
746
747
748
749
750
751
752
753
754
755
756
757
758
759
760
761
762
763
764
765
766
767
768
769
770
771
772
773
774
775
776
777
778
779
779
780
781
782
783
784
785
786
787
788
789
789
790
791
792
793
794
795
796
797
798
799
800
801
802
803
804
805
806
807
808
809
809
810
811
812
813
814
815
816
817
818
819
819
820
821
822
823
824
825
826
827
828
829
829
830
831
832
833
834
835
836
837
838
839
839
840
841
842
843
844
845
846
847
848
849
849
850
851
852
853
854
855
856
857
858
859
859
860
861
862
863
864
865
866
867
868
869
869
870
871
872
873
874
875
876
877
878
879
879
880
881
882
883
884
885
886
887
888
889
889
890
891
892
893
894
895
896
897
898
899
900
901
902
903
904
905
906
907
908
909
909
910
911
912
913
914
915
916
917
918
919
919
920
921
922
923
924
925
926
927
928
929
929
930
931
932
933
934
935
936
937
938
939
939
940
941
942
943
944
945
946
947
948
949
950
951
952
953
954
955
956
957
958
959
959
960
961
962
963
964
965
966
967
968
969
969
970
971
972
973
974
975
976
977
978
979
979
980
981
982
983
984
985
986
987
988
989
989
990
991
992
993
994
995
996
997
998
999
1000
1001
1002
1003
1004
1005
1006
1007
1008
1009
1009
1010
1011
1012
1013
1014
1015
1016
1017
1018
1019
1019
1020
1021
1022
1023
1024
1025
1026
1027
1028
1029
1029
1030
1031
1032
1033
1034
1035
1036
1037
1038
1039
1039
1040
1041
1042
1043
1044
1045
1046
1047
1048
1049
1049
1050
1051
1052
1053
1054
1055
1056
1057
1058
1059
1059
1060
1061
1062
1063
1064
1065
1066
1067
1068
1069
1069
1070
1071
1072
1073
1074
1075
1076
1077
1078
1079
1079
1080
1081
1082
1083
1084
1085
1086
1087
1088
1089
1089
1090
1091
1092
1093
1094
1095
1096
1097
1098
1099
1100
1101
1102
1103
1104
1105
1106
1107
1108
1109
1109
1110
1111
1112
1113
1114
1115
1116
1117
1118
1119
1119
1120
1121
1122
1123
1124
1125
1126
1127
1128
1129
1129
1130
1131
1132
1133
1134
1135
1136
1137
1138
1139
1139
1140
1141
1142
1143
1144
1145
1146
1147
1148
1149
1149
1150
1151
1152
1153
1154
1155
1156
1157
1158
1159
1159
1160
1161
1162
1163
1164
1165
1166
1167
1168
1169
1169
1170
1171
1172
1173
1174
1175
1176
1177
1178
1179
1179
1180
1181
1182
1183
1184
1185
1186
1187
1188
1189
1189
1190
1191
1192
1193
1194
1195
1196
1197
1198
1199
1199
1200
1201
1202
1203
1204
1205
1206
1207
1208
1209
1209
1210
1211
1212
1213
1214
1215
1216
1217
1218
1219
1219
1220
1221
1222
1223
1224
1225
1226
1227
1228
1229
1229
1230
1231
1232
1233
1234
1235
1236
1237
1238
1239
1239
1240
1241
1242
1243
1244
1245
1246
1247
1248
1249
1249
1250
1251
1252
1253
1254
1255
1256
1257
1258
1259
1259
1260
1261
1262
1263
1264
1265
1266
1267
1268
1269
1269
1270
1271
1272
1273
1274
1275
1276
1277
1278
1279
1279
1280
1281
1282
1283
1284
1285
1286
1287
1288
1289
1289
1290
1291
1292
1293
1294
1295
1296
1297
1298
1299
1299
1300
1301
1302
1303
1304
1305
1306
1307
1308
1309
1309
1310
1311
1312
1313
1314
1315
1316
1317
1318
1319
1319
1320
1321
1322
1323
1324
1325
1326
1327
1328
1329
1329
1330
1331
1332
1333
1334
1335
1336
1337
1338
1339
1339
1340
1341
1342
1343
1344
1345
1346
1347
1348
1349
1349
1350
1351
1352
1353
1354
1355
1356
1357
1358
1359
1359
1360
1361
1362
1363
1364
1365
1366
1367
1368
1369
1369
1370
1371
1372
1373
1374
1375
1376
1377
1378
1379
1379
1380
1381
1382
1383
1384
1385
1386
1387
1388
1389
1389
1390
1391
1392
1393
1394
1395
1396
1397
1398
1399
1399
1400
1401
1402
1403
1404
1405
1406
1407
1408
1409
1409
1410
1411
1412
1413
1414
1415
1416
1417
1418
1419
1419
1420
1421
1422
1423
1424
1425
1426
1427
1428
1429
1429
1430
1431
1432
1433
1434
1435
1436
1437
1438
1439
1439
1440
1441
1442
1443
1444
1445
1446
1447
1448
1449
1449
1450
1451
1452
1453
1454
1455
1456
1457
1458
1459
1459
1460
1461
1462
1463
1464
1465
1466
1467
1468
1469
1469
1470
1471
1472
1473
1474
1475
1476
1477
1478
1479
1479
1480
1481
1482
1483
1484
1485
1486
1487
1488
1489
1489
1490
1491
1492
1493
1494
1495
1496
1497
1498
1499
1499
1500
1501
1502
1503
1504
1505
1506
1507
1508
1509
1509
1510
1511
1512
1513
1514
1515
1516
1517
1518
1519
1520
1521
1522
1523
1524
1525
1526
1527
1528
1529
1530
1531
1532
1533
1534
1535
1536
1537
1538
1539
1540
1541
1542
1543
1544
1545
1546
1547
1548
1549
1549
1550
1551
1552
1553
1554
1555
1556
1557
1558
1559
1559
1560
1561
1562
1563
1564
1565
1566
1567
1568
1569
1569
1570
1571
1572
1573
1574
1575
1576
1577
1578
1579
1579
1580
1581
1582
1583
1584
1585
1586
1587
1588
1589
1589
1590
1591
1592
1593
1594
1595
1596
1597
1598
1599
1599
1600
1601
1602
1603
1604
1605
1606
1607
1608
1609
1609
1610
1611
1612
1613
1614
1615
1616
1617
1618
1619
1619
1620
1621
1622
1623
1624
1625
1626
1627
1628
1629
1629
1630
1631
1632
1633
1634
1635
1636
1637
1638
1639
1639
1640
1641
1642
1643
1644
1645
1646
1647
1648
1649
1649
1650
1651
1652
1653
1654
1655
1656
1657
1658
1659
1659
1660
1661
1662
1663
1664
1665
1666
1667
1668
1669
1669
1670
1671
1672
1673
1674
1675
1676
1677
1678
1678
1679
1680
1681
1682
1683
1684
1685
1686
1687
1688
1689
1689
1690
1691
1692
1693
1694
1695
1696
1697
1698
1699
1699
1700
1701
1702
1703
1704
1705
1706
1707
1708
1709
1709
1710
1711
1712
1713
1714
1715
1716
1717
1718
1719
1719
1720
1721
1722
1723
1724
1725
1726
1727
1728
1729
1729
1730
1731
1732
1733
1734
1735
1736
1737
1738
1739
1739
1740
1741
1742
1743
1744
1745
1746
1747
1748
1749
1749
1750
1751
1752
1753
1754
1755
1756
1757
1758
1759
1759
1760
1761
1762
1763
1764
1765
1766
1767
1768
1769
1769
1770
1771
1772
1773
1774
1775
1776
1777
1778
1778
1779
1780
1781
1782
1783
1784
1785
1786
1787
1788
1789
1789
1790
1791
1792
1793
1794
1795
1796
1797
1798
1799
1799
1800
1801
1802
1803
1804
1805
1806
1807
1808
1809
1809
1810
1811
1812
1813
1814
1815
1816
1817
1818
1819
1819
1820
1821
1822
1823
1824
1825
1826
1827
1828
1829
1829
1830
1831
1832
1833
1834
1835
1836
1837
1838
1839
1839
1840
1841
1842
1843
1844
1845
1846
1847
1848
1849
1849
1850
1851
1852
1853
1854
1855
1856
1857
1858
1859
1859
1860
1861
1862
1863
1864
1865
1866
1867
1868
1869
1869
1870
1871
1872
1873
1874
1875
1876
1877
1878
1878
1879
1880
1881
1882
1883
1884
1885
1886
1

540 REFERENCES
541

- 542 Josh Achiam, Steven Adler, Sandhini Agarwal, Lama Ahmad, Ilge Akkaya, Florencia Leoni Aleman,
543 Diogo Almeida, Janko Altenschmidt, Sam Altman, Shyamal Anadkat, et al. Gpt-4 technical report.
544 *arXiv preprint arXiv:2303.08774*, 2023.
- 545 Zafarali Ahmed, Nicolas Le Roux, Mohammad Norouzi, and Dale Schuurmans. Understanding
546 the impact of entropy on policy optimization. In *International conference on machine learning*
547 (*ICML*), 2019.
- 548 Matteo Alleman, Jack Lindsey, and Stefano Fusi. Task structure and nonlinearity jointly deter-
549 mine learned representational geometry. In *The Twelfth International Conference on Learning*
550 *Representations (ICLR)*, 2024.
- 552 John C. Baez. What is entropy? *arXiv preprint arXiv:2409.09232*, 2024. <https://arxiv.org/abs/2409.09232>.
553
- 555 Stella Biderman, Hailey Schoelkopf, Quentin Gregory Anthony, Herbie Bradley, Kyle O'Brien, Eric
556 Hallahan, Mohammad Aflah Khan, Shivanshu Purohit, USVSN Sai Prashanth, Edward Raff, et al.
557 Pythia: A suite for analyzing large language models across training and scaling. In *International*
558 *Conference on Machine Learning (ICML)*, 2023.
- 559 Yelysei Bondarenko, Markus Nagel, and Tijmen Blankevoort. Quantizable transformers: Removing
560 outliers by helping attention heads do nothing. In *Advances in Neural Information Processing*
561 *Systems*, 2023.
- 563 Tom Brown, Benjamin Mann, Nick Ryder, Melanie Subbiah, Jared D Kaplan, Prafulla Dhariwal,
564 Arvind Neelakantan, Pranav Shyam, Girish Sastry, Amanda Askell, et al. Language models are
565 few-shot learners. *Advances in neural information processing systems*, 2020.
- 566 Nicola Cancedda. Spectral filters, dark signals, and attention sinks. In *Proceedings of the 62nd*
567 *Annual Meeting of the Association for Computational Linguistics (ACL)*, 2024.
- 569 Nicholas Carlini, Daniel Paleka, Krishnamurthy Dj Dvijotham, Thomas Steinke, Jonathan Hayase,
570 A Feder Cooper, Katherine Lee, Matthew Jagielski, Milad Nasr, Arthur Conmy, et al. Stealing part
571 of a production language model. In *International Conference on Machine Learning (ICML)*, 2024.
- 573 Dake Chen, Yuke Zhang, Souvik Kundu, Chenghao Li, and Peter A Beerel. Rna-vit: Reduced-
574 dimension approximate normalized attention vision transformers for latency efficient private
575 inference. In *IEEE/ACM International Conference on Computer Aided Design (ICCAD)*, 2023.
- 576 Xiang Cheng, Yuxin Chen, and Suvrit Sra. Transformers implement functional gradient descent to
577 learn non-linear functions in context. In *Forty-first International Conference on Machine Learning*
578 (*ICML*), 2024.
- 579 Mostafa Dehghani, Josip Djolonga, Basil Mustafa, Piotr Padlewski, Jonathan Heek, Justin Gilmer,
580 Andreas Peter Steiner, Mathilde Caron, Robert Geirhos, Ibrahim Alabdulmohsin, et al. Scaling
581 vision transformers to 22 billion parameters. In *International Conference on Machine Learning*
582 (*ICML*), 2023.
- 584 Tim Dettmers and Luke Zettlemoyer. The case for 4-bit precision: k-bit inference scaling laws. In
585 *International Conference on Machine Learning (ICML)*, 2023.
- 586 Naren Dhyani, Jianqiao Mo, Patrick Yubearon, Minsu Cho, Ameya Joshi, Siddharth Garg, Brandon
587 Reagen, and Chinmay Hegde. Privit: Vision transformers for fast private inference. In *Transactions*
588 *on Machine Learning Research (TMLR)*, 2024.
- 590 Nelson Elhage, Robert Lasenby, and Christopher Olah. Privileged bases in the transformer residual
591 stream. *Transformer Circuits Thread*, 2023.
- 593 Hugging Face. Codeparrot. <https://huggingface.co/learn/nlp-course/chapter7/6>.

- 594 Javier Ferrando, Gabriele Sarti, Arianna Bisazza, and Marta R Costa-jussà. A primer on the inner
 595 workings of transformer-based language models. *arXiv preprint arXiv:2405.00208*, 2024.
 596
- 597 Jonas Geiping and Tom Goldstein. Cramming: Training a language model on a single gpu in one day.
 598 In *International Conference on Machine Learning (ICML)*, 2023.
- 599 Hamidreza Ghader and Christof Monz. What does attention in neural machine translation pay
 600 attention to? In *Proceedings of the The 8th International Joint Conference on Natural Language
 601 Processing*, 2017.
- 602 Elliot Glazer, Ege Erdil, Tamay Besiroglu, Diego Chicharro, Evan Chen, Alex Gunning, Caroline Falk-
 603 man Olsson, Jean-Stanislas Denain, Anson Ho, Emily de Oliveira Santos, et al. Frontiermath: A
 604 benchmark for evaluating advanced mathematical reasoning in ai. *arXiv preprint arXiv:2411.04872*,
 605 2024.
- 606 Rhys Gould, Euan Ong, George Ogden, and Arthur Conmy. Successor heads: Recurring, interpretable
 607 attention heads in the wild. In *The Twelfth International Conference on Learning Representations
 608 (ICLR)*, 2024.
- 609 Xiangming Gu, Tianyu Pang, Chao Du, Qian Liu, Fengzhuo Zhang, Cunxiao Du, Ye Wang, and
 610 Min Lin. When attention sink emerges in language models: An empirical view. *arXiv preprint
 611 arXiv:2410.10781*, 2024.
- 612 Yuxian Gu, Li Dong, Furu Wei, and Minlie Huang. Minillm: Knowledge distillation of large language
 613 models. In *The Twelfth International Conference on Learning Representations (ICLR)*, 2023.
- 614 Kanav Gupta, Neha Jawalkar, Ananta Mukherjee, Nishanth Chandran, Divya Gupta, Ashish Panwar,
 615 and Rahul Sharma. SIGMA: secure GPT inference with function secret sharing. In *Proceedings
 616 on Privacy Enhancing Technologies (PETS)*, 2024.
- 617 Wes Gurnee, Neel Nanda, Matthew Pauly, Katherine Harvey, Dmitrii Troitskii, and Dimitris Bertsimas.
 618 Finding neurons in a haystack: Case studies with sparse probing. In *Transactions on Machine
 619 Learning Research (TMLR)*, 2023.
- 620 Wes Gurnee, Theo Horsley, Zifan Carl Guo, Tara Rezaei Kheirkhah, Qinyi Sun, Will Hathaway, Neel
 621 Nanda, and Dimitris Bertsimas. Universal neurons in GPT2 language models. In *Transactions on
 622 Machine Learning Research (TMLR)*, 2024.
- 623 Meng Hao, Hongwei Li, Hanxiao Chen, Pengzhi Xing, Guowen Xu, and Tianwei Zhang. Iron:
 624 Private inference on transformers. In *Advances in Neural Information Processing Systems*, 2022.
- 625 Adi Haviv, Ido Cohen, Jacob Gidron, Roei Schuster, Yoav Goldberg, and Mor Geva. Understanding
 626 transformer memorization recall through idioms. In *Proceedings of the 17th Conference of the
 627 European Chapter of the Association for Computational Linguistics (EACL)*, 2023.
- 628 Bobby He and Thomas Hofmann. Simplifying transformer blocks. In *The Twelfth International
 629 Conference on Learning Representations (ICLR)*, 2024.
- 630 Bobby He, James Martens, Guodong Zhang, Aleksandar Botev, Andrew Brock, Samuel L Smith, and
 631 Yee Whye Teh. Deep transformers without shortcuts: Modifying self-attention for faithful signal
 632 propagation. In *The Eleventh International Conference on Learning Representations (ICLR)*, 2023.
- 633 Bobby He, Lorenzo Noci, Daniele Paliotta, Imanol Schlag, and Thomas Hofmann. Understanding
 634 and minimising outlier features in neural network training. In *Advances in Neural Information
 635 Processing Systems (NeurIPS)*, 2024.
- 636 Xiaoyang Hou, Jian Liu, Jingyu Li, Yuhan Li, Wen-jie Lu, Cheng Hong, and Kui Ren. Ciphergpt:
 637 Secure two-party gpt inference. *Cryptology ePrint Archive*, 2023.
- 638 Cheng-Yu Hsieh, Chun-Liang Li, Chih-Kuan Yeh, Hootan Nakhost, Yasuhisa Fujii, Alexander Ratner,
 639 Ranjay Krishna, Chen-Yu Lee, and Tomas Pfister. Distilling step-by-step! outperforming larger
 640 language models with less training data and smaller model sizes. In *Annual Meeting of the
 641 Association for Computational Linguistics (ACL)*, 2023.

- 648 Chenhui Hu, Pengfei Cao, Yubo Chen, Kang Liu, and Jun Zhao. Wilke: Wise-layer knowledge
 649 editor for lifelong knowledge editing. In *Findings of the Association for Computational Linguistics*
 650 (*ACL*), 2024a.
- 651 Jerry Yao-Chieh Hu, Pei-Hsuan Chang, Haozheng Luo, Hong-Yu Chen, Weijian Li, Wei-Po Wang,
 652 and Han Liu. Outlier-efficient hopfield layers for large transformer-based models. In *Forty-first*
 653 *International Conference on Machine Learning (ICML)*, 2024b.
- 654 DeLesley Hutchins, Imanol Schlag, Yuhuai Wu, Ethan Dyer, and Behnam Neyshabur. Block-recurrent
 655 transformers. In *Advances in neural information processing systems (NeurIPS)*, 2022.
- 656 Yuval Ishai, Joe Kilian, Kobbi Nissim, and Erez Petrank. Extending oblivious transfers efficiently. In
 657 *Annual International Cryptology Conference (CRYPTO)*, 2003.
- 658 Gauri Jagatap, Ameya Joshi, Animesh Basak Chowdhury, Siddharth Garg, and Chinmay Hegde.
 659 Adversarially robust learning via entropic regularization. In *Frontiers in artificial intelligence*,
 660 2022.
- 661 Edwin T Jaynes. Information theory and statistical mechanics. *Physical review*, 1957.
- 662 Edwin T Jaynes. On the rationale of maximum-entropy methods. In *Proceedings of the IEEE*, 1982.
- 663 Fred Jelinek, Robert L Mercer, Lalit R Bahl, and James K Baker. Perplexity—a measure of the
 664 difficulty of speech recognition tasks. *The Journal of the Acoustical Society of America*, 1977.
- 665 Albert Q Jiang, Alexandre Sablayrolles, Arthur Mensch, Chris Bamford, Devendra Singh Chaplot,
 666 Diego de las Casas, Florian Bressand, Gianna Lengyel, Guillaume Lample, Lucile Saulnier, et al.
 667 Mistral 7b. *arXiv preprint arXiv:2310.06825*, 2023.
- 668 Zhuoran Jin, Pengfei Cao, Hongbang Yuan, Yubo Chen, Jie Xin Xu, Huaijun Li, Xiaojian Jiang,
 669 Kang Liu, and Jun Zhao. Cutting off the head ends the conflict: A mechanism for interpreting
 670 and mitigating knowledge conflicts in language models. In *Findings of the Association for*
 671 *Computational Linguistics (ACL)*, 2024.
- 672 Jae-young Jo and Sung-Hyon Myaeng. Roles and utilization of attention heads in transformer-
 673 based neural language models. In *Proceedings of the 58th Annual Meeting of the Association for*
 674 *Computational Linguistics*, 2020.
- 675 Amir Joudaki, Hadi Daneshmand, and Francis Bach. On the impact of activation and normalization
 676 in obtaining isometric embeddings at initialization. In *Advances in Neural Information Processing*
 677 *Systems (NeurIPS)*, 2023.
- 678 Nikola Jovanović, Robin Staab, and Martin Vechev. Watermark stealing in large language models. In
 679 *International Conference on Machine Learning (ICML)*, 2024.
- 680 Connor Kissane, Robert Krzyzanowski, Joseph Isaac Bloom, Arthur Conmy, and Neel Nanda. Inter-
 681 preting attention layer outputs with sparse autoencoders. In *ICML 2024 Workshop on Mechanistic*
 682 *Interpretability*, 2024.
- 683 Brian Knott, Shobha Venkataraman, Awni Hannun, Shubho Sengupta, Mark Ibrahim, and Laurens
 684 van der Maaten. Crypten: Secure multi-party computation meets machine learning. *Advances in*
 685 *Neural Information Processing Systems*, 2021.
- 686 Jongwoo Ko, Sungnyun Kim, Tianyi Chen, and Se-Young Yun. Distillm: Towards streamlined
 687 distillation for large language models. In *International Conference on Machine Learning (ICML)*,
 688 2024.
- 689 Goro Kobayashi, Tatsuki Kurabayashi, Sho Yokoi, and Kentaro Inui. Analyzing feed-forward blocks
 690 in transformers through the lens of attention map. In *The Twelfth International Conference on*
 691 *Learning Representations (ICLR)*, 2024.
- 692 Olga Kovaleva, Saurabh Kulshreshtha, Anna Rogers, and Anna Rumshisky. Bert busters: Outlier
 693 dimensions that disrupt transformers. In *Findings of the Association for Computational Linguistics*
 694 (*ACL-IJCNLP*), 2021.

- 702 Pierre-Carl Langlais. Entropy is all you need? the quest for best tokens and the new physics of llms.
 703 <https://indico.cern.ch/event/1474571/>, 2024.
- 704
- 705 Goode Lauren and Will Knight. Chatgpt can now talk to
 706 you—and look into your life. [https://www.wired.com/story/
 707 chatgpt-can-now-talk-to-you-and-look-into-your-life/](https://www.wired.com/story/chatgpt-can-now-talk-to-you-and-look-into-your-life/), 2023.
- 708 Dacheng Li, Hongyi Wang, Rulin Shao, Han Guo, Eric Xing, and Hao Zhang. MPCFORMER: FAST,
 709 PERFORMANT AND PRIVATE TRANSFORMER INFERENCE WITH MPC. In *The Eleventh
 710 International Conference on Learning Representations (ICLR)*, 2023a.
- 711
- 712 Hongkang Li, Meng Wang, Songtao Lu, Xiaodong Cui, and Pin-Yu Chen. How do nonlinear
 713 transformers learn and generalize in in-context learning? In *Forty-first International Conference
 714 on Machine Learning (ICML)*, 2024.
- 715 Liunian Harold Li, Jack Hessel, Youngjae Yu, Xiang Ren, Kai-Wei Chang, and Yejin Choi. Symbolic
 716 chain-of-thought distillation: Small models can also "think" step-by-step. In *Annual Meeting of
 717 the Association for Computational Linguistics (ACL)*, 2023b.
- 718
- 719 Zheng Li, Soroush Ghodrati, Amir Yazdanbakhsh, Hadi Esmaeilzadeh, and Mingu Kang. Accelerating
 720 attention through gradient-based learned runtime pruning. In *Proceedings of the 49th Annual
 721 International Symposium on Computer Architecture (ISCA)*, 2022.
- 722 Chen Liang, Simiao Zuo, Qingru Zhang, Pengcheng He, Weizhu Chen, and Tuo Zhao. Less is more:
 723 Task-aware layer-wise distillation for language model compression. In *International Conference
 724 on Machine Learning (ICML)*, 2023.
- 725
- 726 Wen-jie Lu, Zhicong Huang, Zhen Gu, Jingyu Li, Jian Liu, Kui Ren, Cheng Hong, Tao Wei, and
 727 WenGuang Chen. Bumblebee: Secure two-party inference framework for large transformers. In
 728 *Annual Network and Distributed System Security Symposium (NDSS)*, 2025.
- 729
- 730 Xin Lu, Yanyan Zhao, and Bing Qin. How does architecture influence the base capabilities of
 731 pre-trained language models? a case study based on ffn-wider transformer models. In *Advances in
 732 Neural Information Processing Systems (NeurIPS)*, 2024.
- 733
- 734 Xiuyuan Lu and Benjamin Van Roy. Information-theoretic confidence bounds for reinforcement
 735 learning. In *Advances in Neural Information Processing Systems*, 2019.
- 736
- 737 Weicheng Ma, Kai Zhang, Renze Lou, Lili Wang, and Soroush Vosoughi. Contributions of transformer
 738 attention heads in multi- and cross-lingual tasks. In *Annual Meeting of the Association for
 739 Computational Linguistics (ACL)*, 2021.
- 740
- 741 Andrew L Maas, Awni Y Hannun, Andrew Y Ng, et al. Rectifier nonlinearities improve neural
 742 network acoustic models. In *International Conference on Machine Learning (ICML)*, 2013.
- 743
- 744 Kevin Meng, David Bau, Alex Andonian, and Yonatan Belinkov. Locating and editing factual
 745 associations in gpt. In *Advances in Neural Information Processing Systems (NeurIPS)*, 2022.
- 746
- 747 Paul Michel, Omer Levy, and Graham Neubig. Are sixteen heads really better than one? In *Advances
 748 in neural information processing systems*, 2019.
- 749
- 750 David Miller, Ajit V Rao, Kenneth Rose, and Allen Gersho. A global optimization technique for
 751 statistical classifier design. *IEEE transactions on signal processing*, 1996.
- 752
- 753 Niloofar Mireshghallah, Hyunwoo Kim, Xuhui Zhou, Yulia Tsvetkov, Maarten Sap, Reza Shokri,
 754 and Yejin Choi. Can LLMs keep a secret? testing privacy implications of language models via
 755 contextual integrity theory. In *The Twelfth International Conference on Learning Representations*,
 2024.
- 756
- 757 Seyed Iman Mirzadeh, Keivan Alizadeh-Vahid, Sachin Mehta, Carlo C del Mundo, Oncel Tuzel,
 758 Golnoosh Samei, Mohammad Rastegari, and Mehrdad Farajtabar. ReLU strikes back: Exploiting
 759 activation sparsity in large language models. In *The Twelfth International Conference on Learning
 760 Representations (ICLR)*, 2024.

- 756 Takeru Miyato, Toshiki Kataoka, Masanori Koyama, and Yuichi Yoshida. Spectral normalization for
 757 generative adversarial networks. In *International Conference on Learning Representations (ICLR)*,
 758 2018.
- 759 Volodymyr Mnih. Asynchronous methods for deep reinforcement learning. In *Proceedings of The
 760 33rd International Conference on Machine Learning (ICML)*, 2016.
- 762 Jesse Mu and Jacob Andreas. Compositional explanations of neurons. In *Advances in Neural
 763 Information Processing Systems (NeurIPS)*, 2020.
- 764 Yury Nahshan, Joseph Kampeas, and Emir Haleva. Linear log-normal attention with unbiased
 765 concentration. In *The Twelfth International Conference on Learning Representations (ICLR)*, 2024.
- 767 Neel Nanda. Attribution patching: Activation patching at industrial scale. URL: [https://www.
 768 neelnanda.io/mechanistic-interpretability/attribution-patching](https://www.neelnanda.io/mechanistic-interpretability/attribution-patching), 2023.
- 770 Neel Nanda, Senthooran Rajamanoharan, Janos Kramar, and Rohin Shah. Fact finding: Trying
 771 to mechanistically understanding early MLPs. [https://www.alignmentforum.org/s/
 772 hpWHhjvjn67LJ4xXX/p/CW5onXm6uZxpbpsRk](https://www.alignmentforum.org/s/hpWHhjvjn67LJ4xXX/p/CW5onXm6uZxpbpsRk), December 2023.
- 773 Gergely Neu, Anders Jonsson, and Vicenç Gómez. A unified view of entropy-regularized markov
 774 decision processes. *arXiv preprint arXiv:1705.07798*, 2017.
- 775 Yunhao Ni, Yuxin Guo, Junlong Jia, and Lei Huang. On the nonlinearity of layer normalization. In
 776 *Forty-first International Conference on Machine Learning (ICML)*, 2024.
- 778 Lorenzo Noci, Chuning Li, Mufan Li, Bobby He, Thomas Hofmann, Chris J Maddison, and Dan
 779 Roy. The shaped transformer: Attention models in the infinite depth-and-width limit. *Advances in
 780 Neural Information Processing Systems (NeurIPS)*, 2023.
- 781 Qi Pang, Jinhao Zhu, Helen Möllering, Wenting Zheng, and Thomas Schneider. Bolt: Privacy-
 782 preserving, accurate and efficient inference for transformers. In *IEEE Symposium on Security and
 783 Privacy (SP)*, 2024.
- 785 Michael T Pearce, Thomas Dooms, and Alice Rigg. Weight-based decomposition: A case for bilinear
 786 MLPs. In *ICML 2024 Workshop on Mechanistic Interpretability*, 2024.
- 787 David Peer, Bart Keulen, Sebastian Stabinger, Justus Piater, and Antonio Rodriguez-sanchez. Im-
 788 proving the trainability of deep neural networks through layerwise batch-entropy regularization. In
 789 *Transactions on Machine Learning Research (TMLR)*, 2022.
- 791 Gabriel Pereyra, George Tucker, Jan Chorowski, Łukasz Kaiser, and Geoffrey Hinton. Regularizing
 792 neural networks by penalizing confident output distributions. *arXiv preprint arXiv:1701.06548*,
 793 2017.
- 794 NVIDIA Deep Learning Performance. Matrix multiplication background user's
 795 guide. [https://docs.nvidia.com/deeplearning/performance/
 796 dl-performance-matrix-multiplication/index.html](https://docs.nvidia.com/deeplearning/performance/dl-performance-matrix-multiplication/index.html), 2023.
- 798 Telmo Pessoa Pires, António V Lopes, Yannick Assogba, and Hendra Setiawan. One wide feedforward
 799 is all you need. In *Proceedings of the Eighth Conference on Machine Translation*, 2023.
- 800 Aman Priyanshu, Supriti Vijay, Ayush Kumar, Rakshit Naidu, and Fatemehsadat Mireshghallah. Are
 801 chatbots ready for privacy-sensitive applications? an investigation into input regurgitation and
 802 prompt-induced sanitization. *arXiv preprint arXiv:2305.15008*, 2023.
- 804 Alec Radford, Jeffrey Wu, Rewon Child, David Luan, Dario Amodei, Ilya Sutskever, et al. Language
 805 models are unsupervised multitask learners. *OpenAI blog*, 2019.
- 806 Oleg Rybakov, Mike Chrzanowski, Peter Dykas, Jinze Xue, and Ben Lanir. Methods of improving
 807 llm training stability. *arXiv preprint arXiv:2410.16682*, 2024.
- 809 Tim Salimans and Durk P Kingma. Weight normalization: A simple reparameterization to accelerate
 training of deep neural networks. In *Advances in neural information processing systems*, 2016.

- 810 Amrith Setlur, Benjamin Eysenbach, Virginia Smith, and Sergey Levine. Maximizing entropy on
 811 adversarial examples can improve generalization. In *ICLR 2022 Workshop on PAIR^2Struct: Privacy, Accountability, Interpretability, Robustness, Reasoning on Structured Data*, 2022.
- 812
- 813 Claude Elwood Shannon. A mathematical theory of communication. *The Bell system technical journal*, 1948.
- 814
- 815 Pratyusha Sharma, Jordan T. Ash, and Dipendra Misra. The truth is in there: Improving reasoning
 816 with layer-selective rank reduction. In *The Twelfth International Conference on Learning
 817 Representations (ICLR)*, 2024.
- 818
- 819 Robin Staab, Mark Vero, Mislav Balunovic, and Martin Vechev. Beyond memorization: Violating
 820 privacy via inference with large language models. In *The Twelfth International Conference on
 821 Learning Representations (ICLR)*, 2024.
- 822
- 823 Aleksandar Stanić, Dylan Ashley, Oleg Serikov, Louis Kirsch, Francesco Faccio, Jürgen Schmidhuber,
 824 Thomas Hofmann, and Imanol Schlag. The languini kitchen: Enabling language modelling research
 825 at different scales of compute. *arXiv preprint arXiv:2309.11197*, 2023.
- 826
- 827 Alessandro Stolfo, Yonatan Belinkov, and Mrinmaya Sachan. A mechanistic interpretation of
 828 arithmetic reasoning in language models using causal mediation analysis. In *Empirical Methods in
 829 Natural Language Processing (EMNLP)*, 2023.
- 830
- 831 Alessandro Stolfo, Ben Peng Wu, Wes Gurnee, Yonatan Belinkov, Xingyi Song, Mrinmaya Sachan,
 832 and Neel Nanda. Confidence regulation neurons in language models. In *The Thirty-eighth Annual
 833 Conference on Neural Information Processing Systems (NeurIPS)*, 2024.
- 834
- 835 Entropix Development Team. Entropix: Tool for entropy based sampling and parallel cot decoding.
 836 <https://github.com/xjdr-alt/entropix>, 2024.
- 837
- 838 Gemma Team, Thomas Mesnard, Cassidy Hardin, Robert Dadashi, Surya Bhupatiraju, Shreya Pathak,
 839 Laurent Sifre, Morgane Rivière, Mihir Sanjay Kale, Juliette Love, et al. Gemma: Open models
 840 based on gemini research and technology. *arXiv preprint arXiv:2403.08295*, 2024.
- 841
- 842 Hugo Touvron, Thibaut Lavril, Gautier Izacard, Xavier Martinet, Marie-Anne Lachaux, Timothée
 843 Lacroix, Baptiste Rozière, Naman Goyal, Eric Hambro, Faisal Azhar, et al. Llama: Open and
 844 efficient foundation language models. *arXiv preprint arXiv:2302.13971*, 2023.
- 845
- 846 Petar Veličković, Christos Perivolaropoulos, Federico Barbero, and Razvan Pascanu. softmax is not
 847 enough (for sharp out-of-distribution). *arXiv preprint arXiv:2410.01104*, 2024.
- 848
- 849 Jesse Vig and Yonatan Belinkov. Analyzing the structure of attention in a transformer language
 850 model. In *Proceedings of the 2019 ACL Workshop BlackboxNLP: Analyzing and Interpreting
 851 Neural Networks for NLP*, 2019.
- 852
- 853 Elena Voita, David Talbot, Fedor Moiseev, Rico Sennrich, and Ivan Titov. Analyzing multi-head
 854 self-attention: Specialized heads do the heavy lifting, the rest can be pruned. In *Proceedings of the
 855 57th Annual Meeting of the Association for Computational Linguistics (ACL)*, 2019.
- 856
- 857 Kevin Ro Wang, Alexandre Variengien, Arthur Conmy, Buck Shlegeris, and Jacob Steinhardt.
 858 Interpretability in the wild: a circuit for indirect object identification in GPT-2 small. In *The
 859 Eleventh International Conference on Learning Representations (ICLR)*, 2023.
- 860
- 861 Yinuo Wang, Likun Wang, Yuxuan Jiang, Wenjun Zou, Tong Liu, Xujie Song, Wenxuan Wang,
 862 Liming Xiao, Jiang Wu, Jingliang Duan, et al. Diffusion actor-critic with entropy regulator. In
 863 *Advances in Neural Information Processing Systems (NeurIPS)*, 2024.
- 864
- 865 Xiuying Wei, Yunchen Zhang, Xiangguo Zhang, Ruihao Gong, Shanghang Zhang, Qi Zhang, Fengwei
 866 Yu, and Xianglong Liu. Outlier suppression: Pushing the limit of low-bit transformer language
 867 models. In *Advances in Neural Information Processing Systems (NeurIPS)*, 2022.

- 864 Mitchell Wortsman, Peter J Liu, Lechao Xiao, Katie E Everett, Alexander A Alemi, Ben Adlam,
 865 John D Co-Reyes, Izzeddin Gur, Abhishek Kumar, Roman Novak, Jeffrey Pennington, Jascha
 866 Sohl-Dickstein, Kelvin Xu, Jaehoon Lee, Justin Gilmer, and Simon Kornblith. Small-scale proxies
 867 for large-scale transformer training instabilities. In *The Twelfth International Conference on*
 868 *Learning Representations (ICLR)*, 2024.
- 869 Xiaoxia Wu, Cheng Li, Reza Yazdani Aminabadi, Zhewei Yao, and Yuxiong He. Understanding
 870 int4 quantization for language models: latency speedup, composability, and failure cases. In
 871 *International Conference on Machine Learning (ICML)*, 2023.
- 872 Xinyi Wu, Amir Ajourlou, Yifei Wang, Stefanie Jegelka, and Ali Jadbabaie. On the role of attention
 873 masks and layernorm in transformers. In *Advances in Neural Information Processing Systems*
 874 (*NeurIPS*), 2024.
- 875 Guangxuan Xiao, Ji Lin, Mickael Seznec, Hao Wu, Julien Demouth, and Song Han. Smoothquant:
 876 Accurate and efficient post-training quantization for large language models. In *International*
 877 *Conference on Machine Learning (ICML)*, 2023.
- 878 Guangxuan Xiao, Yuandong Tian, Beidi Chen, Song Han, and Mike Lewis. Efficient streaming
 879 language models with attention sinks. In *The Twelfth International Conference on Learning*
 880 *Representations (ICML)*, 2024.
- 881 Ruibin Xiong, Yunchang Yang, Di He, Kai Zheng, Shuxin Zheng, Chen Xing, Huishuai Zhang,
 882 Yanyan Lan, Liwei Wang, and Tieyan Liu. On layer normalization in the transformer architecture.
 883 In *International Conference on Machine Learning (ICML)*, 2020.
- 884 Kang Yang, Chenkai Weng, Xiao Lan, Jiang Zhang, and Xiao Wang. Ferret: Fast extension for
 885 correlated ot with small communication. In *Proceedings of the 2020 ACM SIGSAC Conference on*
 886 *Computer and Communications Security (CCS)*, 2020.
- 887 Tianzhu Ye, Li Dong, Yuqing Xia, Yutao Sun, Yi Zhu, Gao Huang, and Furu Wei. Differential
 888 transformer. In *arXiv preprint arXiv:2410.05258*, 2024.
- 889 Qingyu Yin, Xuzheng He, Xiang Zhuang, Yu Zhao, Jianhua Yao, Xiaoyu Shen, and Qiang Zhang.
 890 Stablemask: Refining causal masking in decoder-only transformer. In *Forty-first International*
 891 *Conference on Machine Learning (ICML)*, 2024.
- 892 Zhongzhi Yu, Zheng Wang, Yonggan Fu, Huihong Shi, Khalid Shaikh, and Yingyan Celine Lin.
 893 Unveiling and harnessing hidden attention sinks: Enhancing large language models without training
 894 through attention calibration. In *Forty-first International Conference on Machine Learning (ICML)*,
 895 2024.
- 896 Wenxuan Zeng, Meng Li, Wenjie Xiong, Wenjie Lu, Jin Tan, Runsheng Wang, and Ru Huang. Mpcvit:
 897 Searching for mpc-friendly vision transformer with heterogeneous attention. In *Proceedings of the*
 898 *IEEE/CVF International Conference on Computer Vision (ICCV)*, 2023.
- 899 Shuangfei Zhai, Tatiana Likhomanenko, Etaı Littwin, Dan Busbridge, Jason Ramapuram, Yizhe
 900 Zhang, Jiatao Gu, and Joshua M Susskind. Stabilizing transformer training by preventing attention
 901 entropy collapse. In *International Conference on Machine Learning (ICML)*, 2023.
- 902 Jiawen Zhang, Jian Liu, Xinpeng Yang, Yinghao Wang, Kejia Chen, Xiaoyang Hou, Kui Ren,
 903 and Xiaohu Yang. Secure transformer inference made non-interactive. In *Annual Network and*
 904 *Distributed System Security Symposium (NDSS)*, 2025.
- 905 Michael Zhang, Kush Bhatia, Hermann Kumbong, and Christopher Re. The hedgehog & the
 906 porcupine: Expressive linear attentions with softmax mimicry. In *The Twelfth International*
 907 *Conference on Learning Representations (ICLR)*, 2024.
- 908 Yuke Zhang, Dake Chen, Souvik Kundu, Chenghao Li, and Peter A. Beerel. Sal-vit: Towards
 909 latency efficient private inference on vit using selective attention search with a learnable softmax
 910 approximation. In *Proceedings of the IEEE/CVF International Conference on Computer Vision*
 911 (*ICCV*), 2023.

- 918 Bingchen Zhao, Haoqin Tu, Chen Wei, Jieru Mei, and Cihang Xie. Tuning LayerNorm in attention:
919 towards efficient multi-modal llm finetuning. In *International Conference on Learning
920 Representations (ICLR)*, 2024.
- 921
- 922 Shanshan Zhao, Mingming Gong, Tongliang Liu, Huan Fu, and Dacheng Tao. Domain generalization
923 via entropy regularization. In *Advances in neural information processing systems (NeurIPS)*, 2020.
- 924 Itamar Zimerman, Moran Baruch, Nir Drucker, Gilad Ezov, Omri Soceanu, and Lior Wolf. Con-
925 verting transformers to polynomial form for secure inference over homomorphic encryption. In
926 *International Conference on Machine Learning (ICML)*, 2024.

927
928
929
930
931
932
933
934
935
936
937
938
939
940
941
942
943
944
945
946
947
948
949
950
951
952
953
954
955
956
957
958
959
960
961
962
963
964
965
966
967
968
969
970
971

972

973

974

975

976

977

978

Appendix

Table of Contents

A Shannon Entropy and Its Application in Transformer LLMs	20
A.1 Why Use Entropy to Evaluate the Impact of Nonlinearities?	20
A.2 Evaluating the Sharpness of Attention Score Distributions Using Entropy	20
A.3 Relationship Between Temperature and Shannon Entropy	21
B Integrations of Entropy Regularization in Loss Function	21
B.1 PyTorch Implementation of Entropy Regularization	21
B.2 Entropy Regularization Algorithm	22
C Design of Experiments	22
C.1 Perplexity as a Reliable Metric to Evaluate the LLMs' Performance	23
C.2 Why Training from Scratch to Study Nonlinearities?	24
C.3 Cryptographic Protocols for Linear and Nonlinear Operations	24
D Additional Results	25
D.1 Learnable Scaling Factors in Scaled-FFN of Softmax-only Architecture	25
D.2 Entropy Dynamics in LLM Architecture with Fewer Nonlinearity	26
D.3 Additional Results for Latency and Communication Savings using AERO	28
D.4 Results on Languini Dataset	28
D.5 Results on Pythia-70M	29
D.6 Performance Comparison of Weight and Spectral Normalization	30
D.7 Training Dynamics in Softmax-only Models with Fewer FFNs	30
D.8 Mitigating Over-Regularization with an Appropriate Threshold Margin	30
E FLOPs Computation for Inference	33
E.1 Distribution of FLOPs in GPT-2 Models	34
E.2 Distribution of FLOPs in Pythia Models	34
F Additional Related Work	36
G Discussion	36
G.1 Linear vs. Non-linear FFNs: Privileged Basis and Rotational Invariance	36
G.2 Early vs. Deeper FFNs	37
H Future Work	37
I AERO Beyond Private Inference: Broader Impact and Promises	37

1015

1016

1017

1018

1019

1020

1021

1022

1023

1024

1025

1026 A SHANNON ENTROPY AND ITS APPLICATION IN TRANSFORMER LLMs 1027

1028 A.1 WHY USE ENTROPY TO EVALUATE THE IMPACT OF NONLINEARITIES? 1029

1030 We use entropy as a metric to study the impact of nonlinearities on the transformer-based LLMs for
1031 the following reasons:

- 1032 • *Quantifying attention distribution:* The attention mechanism lies at the core of transformer
1033 architectures, and by computing the entropy of attention score distributions, we can observe how
1034 nonlinearities influence the spread (or the concentration) of attention scores. Higher entropy implies
1035 a more exploratory behavior, while lower entropy suggests a more focused attention distribution.
- 1036 • *Feature selection:* Nonlinearities, such as ReLU, enhance feature selectivity by amplifying im-
1037 portant features and suppressing less relevant ones (Alleman et al., 2024; Maas et al., 2013). Entropy
1038 can measure this selectivity across layers and heads, providing insights into the model’s
1039 prioritization of information. Previous studies have used entropy to capture layer-wise information
1040 flow in neural networks (Peer et al., 2022).
- 1041 • *Exploration vs. exploitation:* Nonlinear operators like the self-attention mechanism, LayerNorm,
1042 and GELU balance exploration and exploitation by selecting relevant features while considering
1043 a broader context. For instance, heads in the first layer focus on exploration, while those in the
1044 second layer focus on exploitation. (see Figures 5a, 5b, 12a and 12b).
- 1045 • *Systematic assessment:* Prior work Zhang et al. (2024); Nahshan et al. (2024); Zhai et al. (2023);
1046 Vig & Belinkov (2019); Ghader & Monz (2017) also used entropy to analyze the behavior of
1047 transformer-based models; thus, enhancing validity and comparability of our findings.

1048 A.2 EVALUATING THE SHARPNESS OF ATTENTION SCORE DISTRIBUTIONS USING ENTROPY 1049

1050 Shannon’s entropy quantifies the uncertainty in a probability distribution, measuring the amount of
1051 information needed to describe the state of a stochastic system (Shannon, 1948; Jaynes, 1957). For
1052 a probability distribution $P(x)$, the entropy is defined as $\mathbf{E}(P) = -\sum_i P(x_i) \log P(x_i)$. Refer to
1053 (Baez, 2024) for details on entropy.

1054 In a softmax-based attention mechanism, each softmax operation yields an entropy value representing
1055 the sharpness or spread of the attention scores for each query position (Ghader & Monz, 2017; Vig
1056 & Belinkov, 2019). Higher entropy indicates a more uniform distribution of softmax scores, while
1057 lower entropy signifies a more focused distribution on certain features (Nahshan et al., 2024).

1058 Let $\mathbf{A}^{(h,l)} \in \mathbb{R}^{T \times T}$ be the attention matrix of h -th head in l -th layer, and each element in the attention
1059 matrix, $a_{ij}^{(l,h)}$, are attention weights for the i -th query and j -th key, which are non-negative and sum
1060 to one for a query:

$$1062 \mathbf{A}^{(l,h)} = \left[a_{ij}^{(l,h)} \right]_{T \times T}, \quad \text{where} \quad a_{ij}^{(l,h)} \geq 0 \quad \text{and} \quad \sum_{j=1}^T a_{ij}^{(l,h)} = 1 \quad (7)$$

1064 This square matrix is generated by applying the softmax operation over the key length for each query
1065 position as follows (i.e., $\mathbf{X} \in \mathbb{R}^{T \times T}$ $\mathbf{X}_i \in \mathbb{R}^{1 \times T}$):

$$1067 \mathbf{A}^{(h,l)}(\mathbf{X}) = \text{Softmax}\left(\frac{1}{\sqrt{d_k}}(\mathbf{X}\mathbf{W}^Q)(\mathbf{X}\mathbf{W}^K)^\top\right), \quad \text{where} \quad \text{Softmax}(\mathbf{X}_i) = \frac{\exp(x_i)}{\sum_{j=1}^T \exp(x_j)} \quad (8)$$

1070 Thus, each element $a_{ij}^{(l,h)}$ of the attention matrix can be represented as follows:

$$1072 a_{ij}^{(l,h)} = \frac{\exp\left(\frac{1}{\sqrt{d_k}}(\mathbf{X}_i\mathbf{W}^Q)(\mathbf{X}_j\mathbf{W}^K)^\top\right)}{\sum_{k=1}^T \exp\left(\frac{1}{\sqrt{d_k}}(\mathbf{X}_i\mathbf{W}^Q)(\mathbf{X}_k\mathbf{W}^K)^\top\right)}. \quad (9)$$

1075 Following (Zhai et al., 2023), we compute the mean of entropy values across all query positions to
1076 obtain a single entropy value for each head. The entropy $\mathbf{E}^{(l,h)}$ for the h -th head in the l -th layer of
1077 an attention matrix is given by:

$$1078 \mathbf{E}^{(l,h)} = -\frac{1}{T} \sum_{i=1}^T \sum_{j=1}^T a_{ij}^{(l,h)} \log(a_{ij}^{(l,h)} + \epsilon) \quad (10)$$

1080 where ϵ is a small constant added for numerical stability to prevent taking the log of zero.
 1081

1082 A.3 RELATIONSHIP BETWEEN TEMPERATURE AND SHANNON ENTROPY 1083

1084 With the learnable temperature parameters (t), the attention matrix can be expressed as follows:
 1085

$$1086 \mathbf{A}^{(l,h)}(t) = \left[a_{ij}^{(l,h)}(t) \right]_{T \times T}, \text{ where } a_{ij}^{(l,h)}(t) = \frac{\exp\left(\frac{1}{t_i \sqrt{d_k}} (\mathbf{X}_i \mathbf{W}^Q)(\mathbf{X}_j \mathbf{W}^K)^\top\right)}{\sum_{k=1}^T \exp\left(\frac{1}{t_i \sqrt{d_k}} (\mathbf{X}_i \mathbf{W}^Q)(\mathbf{X}_k \mathbf{W}^K)^\top\right)}. \quad (11)$$

1090 Let $z_{ij} = (\mathbf{X}_i \mathbf{W}^Q)(\mathbf{X}_j \mathbf{W}^K)^\top$ represents the logits (attention scores before applying softmax).
 1091

1092 Now, substituting $a_{ij}^{(l,h)}(t)$ into the entropy formula:
 1093

$$1094 \mathbf{E}^{(l,h)}(t) = -\frac{1}{T} \sum_{i=1}^T \sum_{j=1}^T \frac{\exp\left(\frac{1}{t \sqrt{d_k}} z_{ij}\right)}{\sum_{k=1}^T \exp\left(\frac{1}{t \sqrt{d_k}} z_{ik}\right)} \log \left(\frac{\exp\left(\frac{1}{t \sqrt{d_k}} z_{ij}\right)}{\sum_{k=1}^T \exp\left(\frac{1}{t \sqrt{d_k}} z_{ik}\right)} \right).$$

1097 Simplifying the logarithmic term:
 1098

$$1099 \log \left(\frac{\exp\left(\frac{1}{t \sqrt{d_k}} z_{ij}\right)}{\sum_{k=1}^T \exp\left(\frac{1}{t \sqrt{d_k}} z_{ik}\right)} \right) = \frac{1}{t \sqrt{d_k}} z_{ij} - \log \left(\sum_{k=1}^T \exp\left(\frac{1}{t \sqrt{d_k}} z_{ik}\right) \right).$$

1103 Thus, the entropy simplifies to:
 1104

$$1106 \mathbf{E}^{(l,h)}(t) = \frac{1}{T} \sum_{i=1}^T \left(\log \left(\sum_{k=1}^T \exp\left(\frac{1}{t \sqrt{d_k}} z_{ik}\right) \right) - \frac{1}{t \sqrt{d_k}} \sum_{j=1}^T a_{ij}^{(l,h)}(t) z_{ij} \right).$$

1109 Further, it can be simplified as a function of expected value of z_{ij} under the attention distribution:
 1110

$$1112 \mathbf{E}^{(l,h)}(t) = \frac{1}{T} \sum_{i=1}^T \left(\log \left(\sum_{k=1}^T \exp\left(\frac{z_{ik}}{t \sqrt{d_k}}\right) \right) - \frac{1}{t \sqrt{d_k}} \mathbb{E}_{j \sim a_{ij}^{(l,h)}(t)} [z_{ij}] \right) \quad (12)$$

1115 In the above expression (Eq. 12), the first term ($\log \sum$) represents the overall *spread* of the logits
 1116 when scaled by t , and the second term ($\frac{1}{t} \mathbb{E}[z_{ij}]$) represents the expected value of the scaled logits
 1117 under the attention distribution.

1118 Temperature cases when:

- 1120 1. $t > 1$: The scaling factor $\frac{1}{t}$ reduces the influence of the logits z_{ij} , making the softmax distribution
 1121 more uniform. Consequently, the entropy *increases*.
- 1122 2. $t < 1$: The scaling factor $\frac{1}{t}$ increases the influence of the logits z_{ij} , making the softmax
 1123 distribution more peaked. Consequently, the entropy *decreases*.
- 1124 3. $t \rightarrow \infty$: The logits are scaled down to zero, and the softmax becomes a uniform distribution. The
 1125 entropy reaches its maximum value of $\log T$.
- 1126 4. $t \rightarrow 0$: The logits dominate the softmax, and it becomes a one-hot distribution. The entropy
 1127 approaches zero.

1128 B INTEGRATIONS OF ENTROPY REGULARIZATION IN LOSS FUNCTION

1129 B.1 PYTORCH IMPLEMENTATION OF ENTROPY REGULARIZATION

1134 The PyTorch implementation below computes the entropy regularization loss for attention weights in
1135 a transformer model. This regularization ensures a balanced attention distribution, preventing it from
1136 becoming overly concentrated or too diffuse.

PyTorch Implementation 1: Entropy Regularization Loss Calculation

```

1139 1 import torch
1140 2
1141 3 def calculate_entropy_reg_loss(attentions, blocks, seq_len):
1142 4     """
1143 5     Calculate the entropy regularization loss.
1144 6
1145 7     Parameters:
1146 8     attentions (list): A list of attention matrices from different layers.
1147 9     blocks (list): A list of transformer blocks.
1148 10    seq_len (int): The length of the sequence (context length).
1149 11
1150 12    Returns:
1151 13    float: The entropy regularization loss.
1152 14    """
1153 15    entropy_reg_loss = 0
1154 16    max_entropy = torch.log(torch.tensor(seq_len)) # Theoretical maximum
1155 17        entropy
1156 18    fraction = 0.10 # Design hyper-parameter for tolerance margin
1157 19    tolerance_margin = fraction * max_entropy # Set tolerance margin as
1158 20        fraction of the maximum entropy
1159 21
1160 22    for layer_idx, (block, attn_mat) in enumerate(zip(blocks, attentions)):
1161 23
1162 24        reg_threshold_weights = block.attn.reg_threshold_weights # Head-
1163 25            wise learnable parameters to set head-specific threshold
1164 26        ent_val = -torch.sum(attn_mat * torch.log(attn_mat + 1e-9), dim=-1)
1165 27            # Compute entropy averaged over sequence length
1166 28        layer_entropy_reg_loss = 0
1167 29
1168 30        for head_idx in range(block.attn.num_heads):
1169 31            head_entropy = ent_val[:, head_idx, :] # Get head-specific
1170 32                entropy
1171 33            threshold = reg_threshold_weights[head_idx] * max_entropy
1172 34            deviation = torch.abs(head_entropy - threshold)
1173 35            penalty = torch.square(torch.where(deviation > tolerance_margin,
1174 36                deviation, torch.zeros_like(deviation)))
1175 37            layer_entropy_reg_loss += penalty.sum()
1176 38
1177 39            layer_entropy_reg_loss /= block.attn.num_heads
1178 40            entropy_reg_loss += layer_entropy_reg_loss
1179 41
1180 42            entropy_reg_loss /= len(attentions)
1181 43            return entropy_reg_loss
1182 44
1183 45    # Calculate the total loss including entropy regularization
1184 46    lambda_reg = 1e-5 # Hyperparameter for entropy regularization weight
1185 47    entropy_regularization = calculate_entropy_reg_loss(attentions, blocks,
1186 48        seq_len)
1187 49    total_loss = ce_loss + lambda_reg * entropy_regularization

```

B.2 ENTROPY REGULARIZATION ALGORITHM

C DESIGN OF EXPERIMENTS

1186 System setup We use a SecretFlow setup (Lu et al., 2025) with the client and server simulated on two
1187 physically separate machines, each equipped with an AMD EPYC 7502 server with specifications
 of 2.5 GHz, 32 cores, and 256 GB RAM. We measure the *end-to-end* PI latency, including input

1188 **Algorithm 1** Entropy Regularization Loss Computation
1189 **Inputs:** attentions: List of attention matrices, $\Theta(L, H)$ = reg_threshold_weights, T : Sequence length,
1190 λ : Regularization loss weightage, γ : Hyper-parameter for Tolerance margin
1191 **Output:** $\mathcal{L}_{\text{total}}$: Total loss including entropy regularization

```

1:    $\mathcal{L}_{\text{entropy}} \leftarrow 0$ 
2:    $E_{\text{max}} \leftarrow \log(T)$                                  $\triangleright$  Theoretical maximum value of entropy
3:    $\text{Tol}_{\text{margin}} \leftarrow \gamma E_{\text{max}}$                  $\triangleright$  Tolerance margin is set as a small fraction of  $E_{\text{max}}$ 
4:   for each layer  $l$  in layers do
5:      $\mathcal{L}_{\text{layer}} \leftarrow 0$ 
6:      $A(t) \leftarrow \text{attentions}[l]$   $\triangleright$  Attention matrix with learnable temperature for each query position
7:      $E(t) \leftarrow -\frac{1}{T} \sum_{i=1}^T \sum_{j=1}^T A_{ij}(t) \log(A_{ij}(t))$   $\triangleright$  Compute entropy, averaged over query length
8:     for each head  $h$  in heads do
9:        $E^{(l,h)} \leftarrow \text{Slice}(E(t), h)$                                  $\triangleright$  Entropy for head  $h$ 
10:       $\theta^{(l,h)} \leftarrow \text{Slice}(\Theta(L, H), h)$                        $\triangleright$  Learnable threshold weight head  $h$ 
11:       $\delta^{(l,h)} \leftarrow E^{(l,h)}(t) - \theta^{(l,h)} E_{\text{max}}$              $\triangleright$  Deviation from head-specific threshold
12:       $\text{penalty}^{(l,h)} \leftarrow (\delta^{(l,h)})^2 \mathbb{1}(|\delta^{(l,h)}| > \text{Tol}_{\text{margin}})$   $\triangleright$  Penalize iff deviation exceeds Tolerance
13:       $\mathcal{L}_{\text{layer}} \leftarrow \mathcal{L}_{\text{layer}} + \text{penalty}^{(l,h)}$ 
14:    end for
15:     $\mathcal{L}_{\text{layer}} \leftarrow \frac{\mathcal{L}_{\text{layer}}}{\text{num\_heads}}$                                  $\triangleright$  Average over heads
16:     $\mathcal{L}_{\text{entropy}} \leftarrow \mathcal{L}_{\text{entropy}} + \mathcal{L}_{\text{layer}}$ 
17:  end for
18:   $\mathcal{L}_{\text{entropy}} \leftarrow \frac{\mathcal{L}_{\text{entropy}}}{\text{len(attentions)}}$                                  $\triangleright$  Average over layers
19:   $\mathcal{L}_{\text{total}} \leftarrow \mathcal{L}_{\text{CE}} + \lambda \mathcal{L}_{\text{entropy}}$ 
20:  return  $\mathcal{L}_{\text{total}}$ 

```

1214 embeddings and final output (vocabulary projection) layers, in WAN setting (bandwidth:100Mbps,
1215 latency:80ms), simulated using Linux Traffic Control (tc) commands. The number of threads is set
1216 to 32. Following He & Hofmann (2024); Stanić et al. (2023); Geiping & Goldstein (2023), all the
1217 models are trained on a single RTX 3090 GPU.

1218 **Datasets** We train models from scratch using the CodeParrot Face and Languini book Stanić et al.
1219 (2023) datasets. The CodeParrot dataset, sourced from 20 million Python files on GitHub, contains 8
1220 GB of files with 16.7 million examples, each with 128 tokens, totaling 2.1 billion training tokens.
1221 We use a tokenizer with a vocabulary of 50K and train with context lengths of 128 and 256. The
1222 Languini book dataset includes 84.5 GB of text from 158,577 books, totaling 23.9 billion tokens with
1223 a WikiText-trained vocabulary of 16,384, and train with context length of 512. Each book averages
1224 559 KB of text or about 150K tokens, with a median size of 476 KB or 128K tokens.

1225 **Training Hyperparameters** For pre-training on the CodeParrot dataset, we adopt the training settings
1226 from (He & Hofmann, 2024). Similarly, for training on the Languini dataset, we follow the settings
1227 from (Stanić et al., 2023). These settings remain consistent across all architectural variations to
1228 accurately reflect the impact of the architectural changes. When applying entropy regularization on
1229 the CodeParrot dataset, we initialize the learnable temperature to 1e-2 and set λ to 1e-5. For the
1230 Languini dataset, the temperature is initialized to 1e-1, and λ is set to 5e-5.

1232 C.1 PERPLEXITY AS A RELIABLE METRIC TO EVALUATE THE LLMs' PERFORMANCE

1234 Perplexity (Jelinek et al., 1977) is a widely adopted metric to evaluate the predictive performance of
1235 auto-regressive language models, reflecting the model's ability to predict the next token in a sequence.
1236 However, for perplexity to serve as a meaningful comparative metric across different architectures,
1237 it is critical to ensure consistency in the tokenizer, and vocabulary size and quality (Hutchins et al.,
1238 2022). Any variation in these components can potentially skew the results by inflating or deflating
1239 perplexity scores; thus, obfuscating the true effects of architectural changes.

1240 In our work, we maintain tokenization schemes and vocabulary attributes as invariant factors across all
1241 experiments within a dataset. This isolation of architectural modifications ensures that any observed
1242 variations in perplexity are directly attributable to changes in the model design. Thus, by enforcing a

consistent tokenization scheme and vocabulary within a dataset, we ensure that perplexity remains a reliable metric for comparing model architectures. Consequently, lower perplexity in our evaluations reliably reflects improved token-level predictions.

C.2 WHY TRAINING FROM SCRATCH TO STUDY NONLINEARITIES?

Understanding the intricate roles of architectural components and nonlinearities—such as activation functions (e.g., GELU, ReLU) in FFN, normalization layers (e.g., LayerNorm), etc.—in transformer-based language models necessitates a methodical and detailed investigative approach. Training models from scratch is essential for this purpose, as it allows us to delve into the internal mechanisms of the model using quantitative measures like entropy. Below, we present a justification for our methodology:

- *Nonlinearities' impact on the fundamental learning dynamics:* Nonlinearities significantly influence the optimization landscape by affecting gradient flow and the model's ability to navigate non-convex loss surfaces. Training models from scratch allow us to observe the fundamental learning dynamics that emerge during the initial stages of training. Thus, constructing models with controlled variations, such as substituting or excluding specific nonlinearities, enables us to isolate their direct effects impact on convergence behavior and training stability.
- *Understanding internal mechanisms through entropy analysis:* Training from scratch enables us to navigate the evolution of entropy values across the layers and assess how architectural components influence information flow within the model. This analysis provides deep insights into the internal workings of models that may not be accessible when starting from pre-trained checkpoints.
- *Limitations of fine-tuning approaches:* The aforementioned granular level of analysis is unattainable when starting from pre-trained models, where the optimization trajectory has already been largely determined. In contrast, training models from scratch eliminates confounding variables that could arise from pre-existing weights and learned representations, ensuring that any observed effects are solely due to the architectural modifications introduced.

C.3 CRYPTOGRAPHIC PROTOCOLS FOR LINEAR AND NONLINEAR OPERATIONS

Linear Operations (MatMul) For privacy-preserving matrix multiplication operations, BumbleBee leverages homomorphic encryption with a novel ciphertext compression strategy Lu et al. (2025). The protocol implements Oblivious Linear Transform (OLT) with efficient packing techniques that reduce communication costs by 80-90% compared to previous approaches. Testing on BERT-base model showed 92% less communication compared to IRON Hao et al. (2022) and 90% less than BOLT Pang et al. (2024). The protocol seamlessly handles both scenarios where one matrix is in plaintext and another is secret-shared, as well as when both matrices are secret-shared, adapting its compression strategy based on matrix dimensions.

GELU To efficiently compute GELU activation, the protocol employs strategic polynomial approximations (with degree 3 and degree 6) across different input ranges. The implementation optimizes branch selection through batched comparisons and leverages mixed bitwidth arithmetic, achieving 89% reduction in communication costs compared to previous approaches. This optimization maintains model accuracy within 1% of plaintext evaluation while being 35% faster in computation time compared to BOLT's implementation.

ReLU The private ReLU is implemented through a composition of secure comparison and multiplexer operations. Using optimized OT(oblivious transfer)-based comparison protocols and Boolean-to-arithmetic conversions, achieving significant efficiency gains. The protocol leverages Ferret OT Yang et al. (2020) instead of traditional IKNP OT Ishai et al. (2003), contributing to the overall improvement in communication efficiency while maintaining the simplicity of ReLU computation.

LayerNorm The LayerNorm computation breaks down into optimized sub-components: secure mean calculation, variance computation using an efficient square protocol, and normalization using reciprocal square root. The implementation takes advantage of squaring operations costing half of general multiplication in secure computation. This optimization, combined with efficient reciprocal computation, shows significant improvement over IRON's approach Hao et al. (2022), contributing to the overall **13 \times** speedup in end-to-end inference time.

1296 **Softmax** For Softmax computation, the protocol implements a numerically stable approach using max
 1297 normalization. The exponential function computation is optimized specifically for negative inputs
 1298 using Taylor approximation, reducing communication by 80% compared to previous approaches. The
 1299 division operation is restructured to use reciprocal followed by multiplication, resulting in over 80%
 1300 reduction in communication costs while maintaining numerical precision.

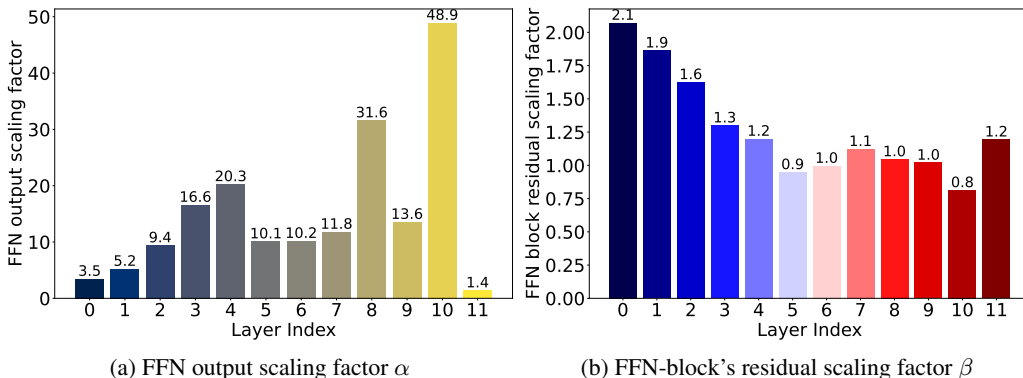
1301 For detailed protocol specifications and security proofs, refer to the BumbleBee paper Lu et al. (2025).
 1302
 1303
 1304

D ADDITIONAL RESULTS

D.1 LEARNABLE SCALING FACTORS IN SCALED-FFN OF SOFTMAX-ONLY ARCHITECTURE

We plot the values of FFN scaling factors α and β (see Eq. 6) learned across the layers in the full-trained softmax-only GPT-2 model, and made the following observations from the Figure 11:

- **Significant increase in α with layer depth:** The scaling factor α increases substantially in the deeper layers of the model, with particularly high values observed in L10. This indicates that as the network goes deeper, the FFN outputs are heavily scaled down by α . This downscaling is essential to prevent the FFN outputs from dominating the activations, which could otherwise lead to numerical instability, as evidenced by the NaNs observed early in training in Figure 6a. The large α values in deeper layers suggest that this downscaling becomes increasingly critical as the model progresses through its layers, effectively stabilizing the training process by keeping the FFN outputs in check.
- **Balancing β values across layers:** The β scaling factors, which modulate the residual connections within the FFN sub-block by up-scaling their output, start higher in the earlier layers and gradually decrease, with some fluctuation, as the layers deepen. The moderate up-scaling provided by β helps to ensure that the residual connections are not overshadowed by the scaled-down FFN outputs. This balance between the strong downscaling by α and the corresponding upscaling by β is crucial for maintaining stable activations across layers, particularly in deeper layers where instability is most likely to occur.



1329 Figure 11: Learned scaling factors α and β in Eq. 6 across different layers in the Softmax-only
 1330 GPT-2 model ($L=12$, $H=12$, $d=768$). The values were plotted after full model training to observe the
 1331 modulation of FFN outputs and residual connections in each layer.
 1332
 1333
 1334
 1335
 1336
 1337
 1338
 1339

1340 These observations underscore the critical role that the learnable scaling factors α and β play in
 1341 stabilizing the training of softmax-only GPT-2 models. By dynamically adjusting the contributions of
 1342 the FFN sub-block outputs, α and β prevent the numerical issues that arise in deeper layers, ensuring
 1343 stable and effective training. This fine-tuned balance is key to avoiding entropy collapse and other
 1344 forms of instability that would otherwise derail the training process.
 1345

1350 **D.2 ENTROPY DYNAMICS IN LLM ARCHITECTURE WITH FEWER NONLINEARITY**
 1351

1352 Figure 12 presents the entropy dynamics of the GPT-2 model as nonlinearities are progressively
 1353 removed, with the models trained from scratch. In Figure 13, the entropy dynamics are shown for a
 1354 normalization-free GPT-2 model with a learnable negative slope in leaky ReLU of FFN. Figure 14
 1355 represents the entropy dynamics when various methods of mitigating the training instability (weight
 1356 and spectral normalization in FFN, and learnable scaling factors for FFN outputs) in Softmax-only
 1357 GPT-2 modes are applied, and also for entropy-regularization which is applied to overcome the
 1358 entropic overload.

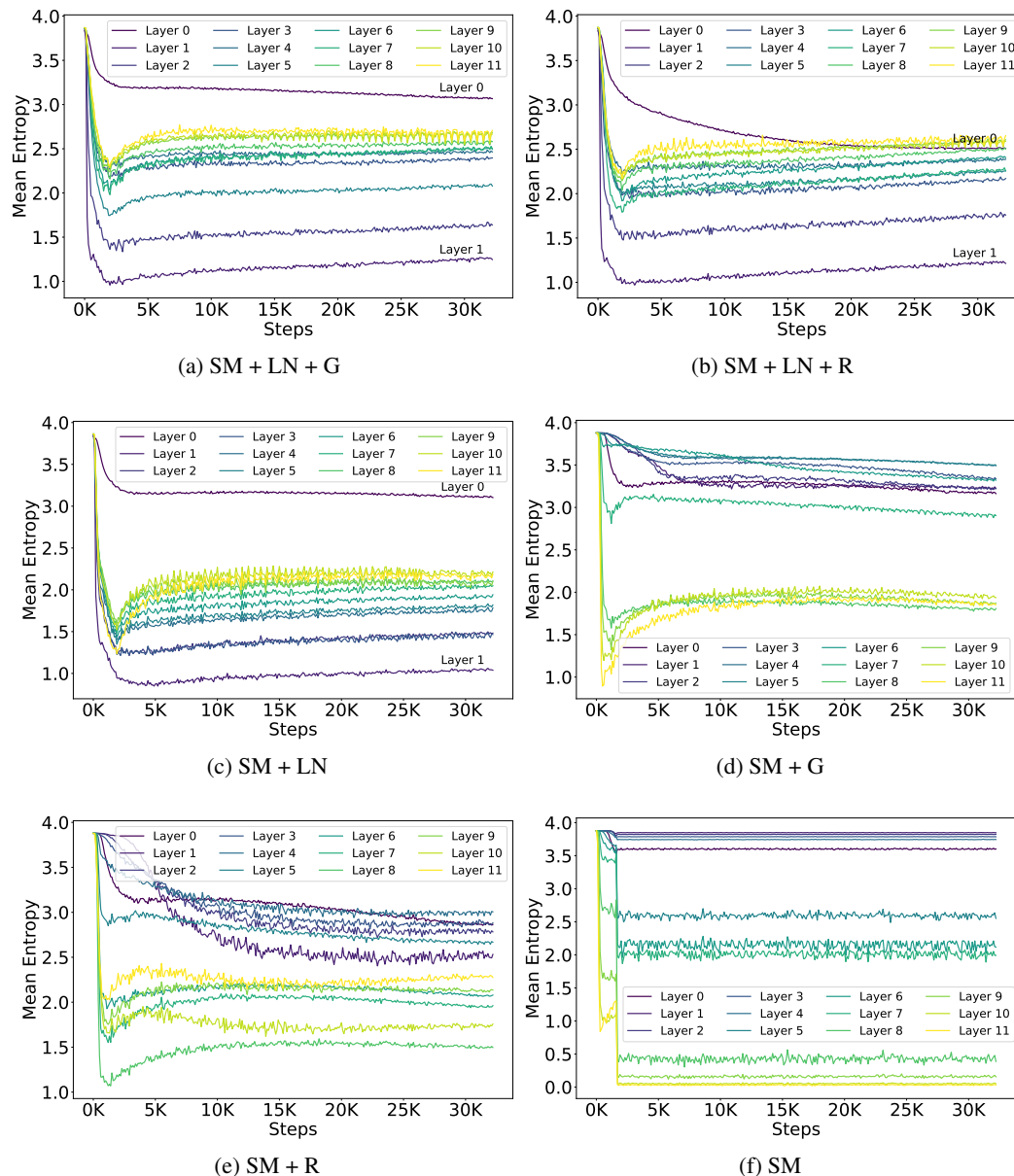


Figure 12: Evolution of Layerwise entropy when GPT-2 ($L=12, H=12, d=768$) models with various nonlinearity configurations are trained from scratch on CodeParrot dataset.

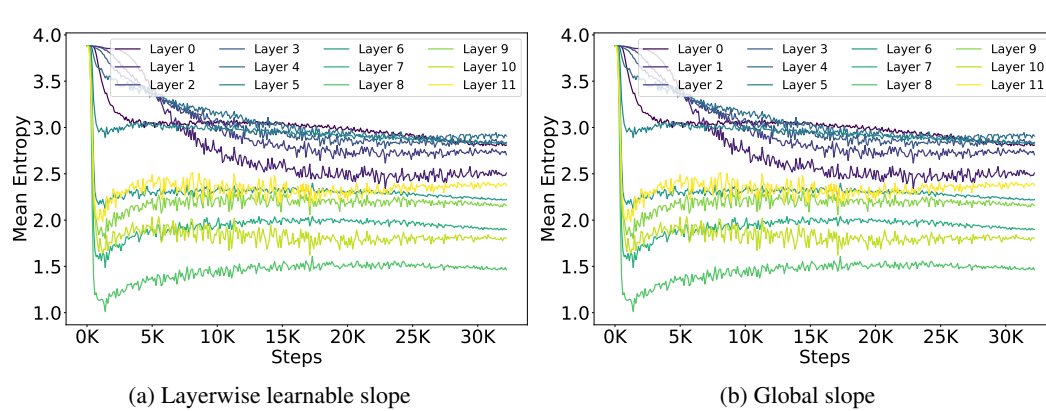


Figure 13: Evolution of layerwise entropy in LayerNorm-free GPT-2 models ($L = 12, H = 12, d = 768$) with a learnable negative slope in the leaky ReLU activation function, trained from scratch on the CodeParrot dataset

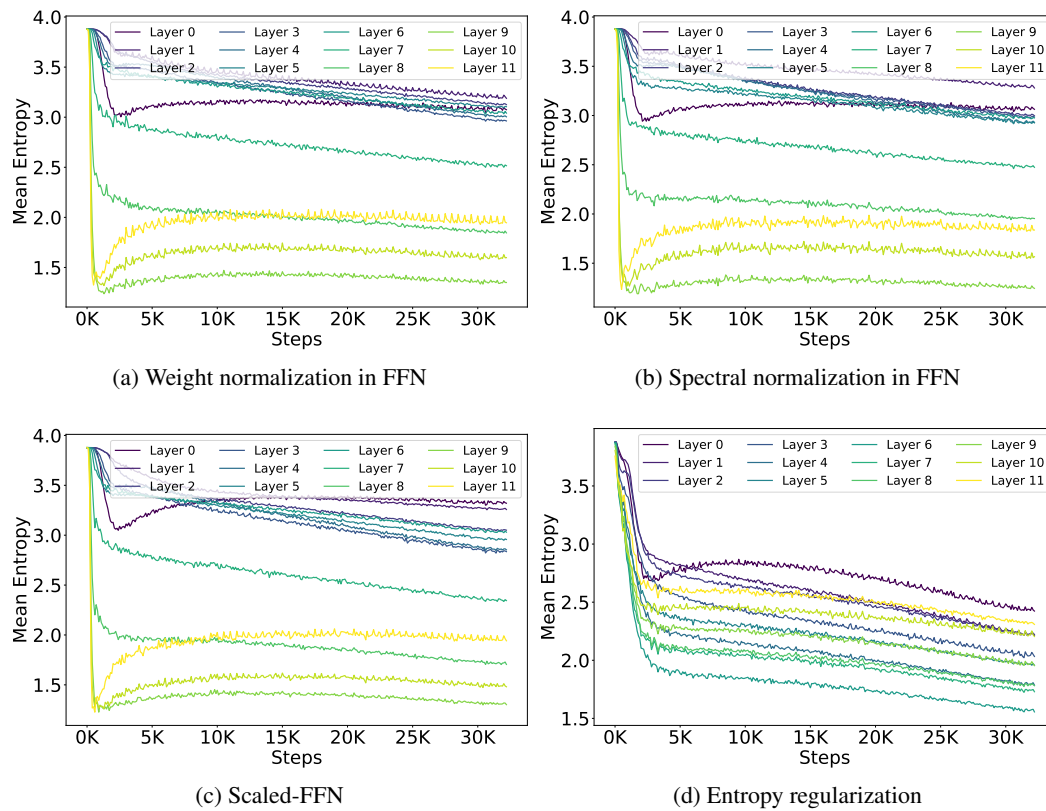


Figure 14: "Layerwise entropy evolution in Softmax-only GPT-2 models ($L = 12, H = 12, d = 768$), trained from scratch on the CodeParrot dataset. Weight and spectral normalization techniques, along with learnable scaling factors (scaled-FFN), are applied in the FFN. In the final configuration (d), entropy regularization is used within the scaled-FFN to address the entropic overload observed in early layers. Notably, the entropy in early layers of (d) is lower compared to (a), (b), and (c).

1458 D.3 ADDITIONAL RESULTS FOR LATENCY AND COMMUNICATION SAVINGS USING AERO
14591460 **GPT-2 Model with 256 tokens as input context** Table 5 provides an analysis of the latency and
1461 communication savings achieved by applying AERO to the GPT-2 model with 256 context length,
1462 along with a detailed breakdown of the nonlinear operations and FLOPs. The performance of AERO
1463 is also compared against SOTA.1464 Table 5: Results, and comparison against SOTA (He & Hofmann, 2024), when GPT-2 ($L=12$, $H=12$,
1465 $d=768$) model is trained from scratch on CodeParrot (Face) dataset with context length 256. NaNs
1466 indicate training instability in SOTA.
1467

	Network Arch.	PPL	#Nonlinear Ops	#FLOPs		Comm. (GB)	Lat. (min.)	Savings	
				FFN	Attn.			Comm.	Lat.
Baseline	SM + LN + G	2.35	SM:144 $\times \mathbb{R}^{256 \times 256}$ LN:24 $\times \mathbb{R}^{256 \times 768}$ G:12 $\times \mathbb{R}^{256 \times 3072}$	29.0B	16.3B	58.51	16.57	1×	1×
	SM + LN + R	2.41	SM:144 $\times \mathbb{R}^{256 \times 256}$ LN:24 $\times \mathbb{R}^{256 \times 768}$ R:12 $\times \mathbb{R}^{256 \times 3072}$	29.0B	16.3B	26.73	12.59	2.19×	1.32×
SOTA	SM + ScFFN	3.47	SM:144 $\times \mathbb{R}^{256 \times 256}$ LN: 1 $\times \mathbb{R}^{256 \times 768}$	29.0B	8.5B	21.52	11.42	2.72×	1.45×
	SM + ScFuFFN	NaN	SM:144 $\times \mathbb{R}^{256 \times 256}$ LN: 1 $\times \mathbb{R}^{256 \times 768}$	3.6B	8.5B	20.48	10.14	2.86×	1.63×
AERO	SM + ScFFN	3.04	SM:144 $\times \mathbb{R}^{256 \times 256}$	29.0B	16.3B	21.77	11.91	2.69×	1.39×
	SM + ScFuFFN	3.03	SM:144 $\times \mathbb{R}^{256 \times 256}$	3.6B	16.3B	20.72	10.45	2.82×	1.59×
	SM + ScFuFFNi ₆	3.08	SM:144 $\times \mathbb{R}^{256 \times 256}$	1.8B	16.3B	20.59	10.32	2.84×	1.61×
	EReg(SM(t) + ScFuFFN)	2.92	SM:144 $\times \mathbb{R}^{256 \times 256}$	3.6B	16.3B	20.72	10.45	2.82×	1.59×
	EReg(SM(t) + ScFuFFNi ₆)	2.97	SM:144 $\times \mathbb{R}^{256 \times 256}$	1.8B	16.3B	20.59	10.32	2.84×	1.61×

1483 **GPT-2 Model with 18 Layers** Table 6 provides an analysis of the latency and communication savings
1484 achieved by applying AERO to the 18-layer GPT-2 model, along with a detailed breakdown of the
1485 nonlinear operations and FLOPs. The performance of AERO is also compared against SOTA.
14861487 Table 6: Results, and comparison against SOTA (He & Hofmann, 2024), when GPT-2 ($L=18$, $H=12$,
1488 $d=768$) model is trained from scratch on CodeParrot (Face) dataset with context length 128. NaNs
1489 indicate training instability in SOTA.
1490

	Network Arch.	PPL	#Nonlinear Ops	#FLOPs		Comm. (GB)	Lat. (min.)	Savings	
				FFN	Attn.			Comm.	Lat.
Baseline	SM + LN + G	2.56	SM:216 $\times \mathbb{R}^{128 \times 128}$ LN:36 $\times \mathbb{R}^{128 \times 768}$ G:18 $\times \mathbb{R}^{128 \times 3072}$	21.7B	11.6B	37.17	10.77	1×	1×
	SM + LN + R	2.63	SM:216 $\times \mathbb{R}^{128 \times 128}$ LN:36 $\times \mathbb{R}^{128 \times 768}$ R:18 $\times \mathbb{R}^{128 \times 3072}$	21.7B	11.6B	13.34	8.04	2.79×	1.34×
SOTA	SM + ScFFN	NaN	SM:216 $\times \mathbb{R}^{128 \times 128}$ LN: 1 $\times \mathbb{R}^{128 \times 768}$	21.7B	5.9B	9.39	6.75	3.96×	1.60×
	SM + ScFuFFN	3.26	SM:216 $\times \mathbb{R}^{128 \times 128}$	21.7B	11.6B	9.62	7.23	3.86×	1.49×
AERO	SM + ScFuFFN	3.24	SM:216 $\times \mathbb{R}^{128 \times 128}$	2.7B	11.6B	8.83	6.07	4.21×	1.77×
	SM + ScFuFFNi ₄	3.27	SM:216 $\times \mathbb{R}^{128 \times 128}$	2.1B	11.6B	8.79	5.85	4.23×	1.84×
	EReg(SM(t) + ScFuFFN)	3.13	SM:216 $\times \mathbb{R}^{128 \times 128}$	2.7B	11.6B	8.83	6.07	4.21×	1.77×
	EReg(SM(t) + ScFuFFNi ₄)	3.17	SM:216 $\times \mathbb{R}^{128 \times 128}$	2.1B	11.6B	8.79	5.85	4.23×	1.84×

1504
1505 D.4 RESULTS ON LANGUINI DATASET
15061507 Table 7 provides an analysis of the latency and communication savings achieved by applying AERO
1508 to the GPT-2 model on Languini dataset, trained on 1.2B, 2.4B, and 4.8B tokens. We also provides a
1509 detailed breakdown of the nonlinear operations and FLOPs.
1510

Table 7: Results, and comparison against SOTA (He & Hofmann, 2024), when GPT-2 ($L=12, H=12, d=768$) model is trained from scratch on Languini (Stanić et al., 2023) dataset with context length 512. NaNs indicate training instability in SOTA.

Network Arch.	Eval PPL			#Nonlinear Ops	#FLOPs		Comm. (GB)	Lat. (min.)	
	1.2B	2.4B	4.8B		FFN	Attn.			
Baseline	SM + LN + G	25.71	23.32	21.29	SM:144 × $\mathbb{R}^{512 \times 512}$ LN:24 × $\mathbb{R}^{512 \times 768}$ G:12 × $\mathbb{R}^{512 \times 3072}$	58.0B	36.2B	145.24	30.74
	SM + LN + R	26.06	23.55	21.58	SM:144 × $\mathbb{R}^{512 \times 512}$ LN:24 × $\mathbb{R}^{512 \times 768}$ R:12 × $\mathbb{R}^{512 \times 3072}$	58.0B	36.2B	81.71	23.54
SOTA	SM + ScFFN	NanNs	NanNs	NanNs	SM:144 × $\mathbb{R}^{512 \times 512}$ LN: 1 × $\mathbb{R}^{512 \times 768}$	58.0B	19.3B	72.10	21.56
AERO	SM + ScFFN	33.91	31.12	28.89	SM:144 × $\mathbb{R}^{512 \times 512}$	58.0B	36.2B	71.76	21.51
	SM + ScFuFFN	33.77	30.82	28.59	SM:144 × $\mathbb{R}^{512 \times 512}$	7.3B	36.2B	69.68	19.44
	SM + ScFuFFNi ₁	34.16	31.23	29.69	SM:144 × $\mathbb{R}^{512 \times 512}$	6.6B	36.2B	69.64	19.11
	EReg(SM(t) + ScFuFFN)	31.54	28.70	26.55	SM:144 × $\mathbb{R}^{512 \times 512}$	7.3B	36.2B	69.68	19.44
	EReg(SM(t) + ScFuFFNi ₁)	31.75	28.93	26.74	SM:144 × $\mathbb{R}^{512 \times 512}$	6.6B	36.2B	69.64	19.11

D.5 RESULTS ON PYTHIA-70M

Table 8 presents the pre-training performance, measured in terms of perplexity, for input context lengths of 128 and 256. The results show the impact of progressively removing nonlinearities from the Pythia-70M model.

Table 8: Results for nonlinearity reduction in Pythia-70M ($L=6, H=8, d=512$) on CodeParrot dataset. LN-free architecture with ReLU activations in FFN (i.e., SM + R) significantly outperform their GELU counterpart (i.e., SM + G) across various content length (T).

	$T=128$		$T=256$	
	Eval PPL	+Δ(%)	Eval PPL	+Δ(%)
SM+LN+G	3.512	0.00	3.054	0.00
SM+LN+R	3.590	2.22	3.107	1.73
SM+LN	4.445	26.56	3.836	25.60
SM+G	4.086	16.35	3.570	16.87
SM+R	3.736	6.36	3.273	7.17

Figure 15 illustrates the step-wise latency and communication savings achieved by applying AERO, as well as its impact on perplexity, on Pythia-70M models, also, compares with the SOTA at iso-latencies.

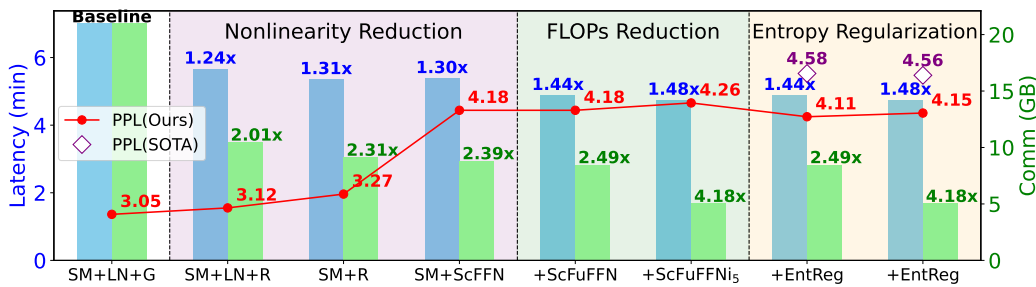


Figure 15: Latency and communication savings through nonlinearity and FLOPs reduction steps when AERO is applied on Pythia-70M, and model is trained from scratch on CodeParrot dataset with context length 256. Further, we benchmark AERO against the SOTA He & Hofmann (2024) at iso-latency points.

1566 D.6 PERFORMANCE COMPARISON OF WEIGHT AND SPECTRAL NORMALIZATION
 1567

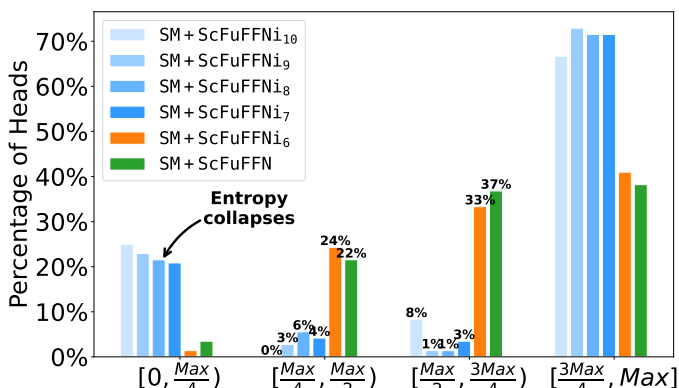
1568 Table 9 compares the performance of weight and spectral normalization applied in various linear
 1569 layers within the attention and FFN sub-blocks. The results show that applying these techniques to
 1570 the attention blocks yields diminishing returns compared to their application in the FFN.
 1571

1572 Table 9: Comparison of weight normalization Salimans & Kingma (2016) and spectral normalization
 1573 Miyato et al. (2018) when employed in Softmax-only GPT-2 ($L=12$, $H=12$, $d=768$) models, and
 1574 trained from scratch on CodeParrot dataset with 128 input context length. FFN weight normalization
 1575 yield the similar results; whereas, weight normalization works better in other linear layers.
 1576

Linear layers	Eval PPL(WNorm)	Eval PPL(SNorm)
QK	3.89	4.25
FFN	3.64	3.63
QK+FFN	3.88	4.23
QKV+FFN	3.93	4.26
QKVO+FFN	3.98	4.34

1583
 1584 D.7 TRAINING DYNAMICS IN SOFTMAX-ONLY MODELS WITH FEWER FFNs
 1585

1586 To further reduce the FLOPs in the
 1587 SM + ScFuFFN model, where each
 1588 FFN is simplified to a single fused
 1589 linear layer, we experimented with
 1590 gradually pruning the deeper FFNs
 1591 by replacing them with identity
 1592 connections and monitoring training
 1593 stability. Figure 16 presents a com-
 1594 parison of headwise entropy distri-
 1595 butions between the pruned and un-
 1596 pruned models, both trained from
 1597 scratch. Instability emerged when
 1598 more than 6 deeper FFNs were
 1599 pruned, as indicated by a signif-
 1600 icant shift in the headwise entropy
 1601 distribution. Specifically, we ob-
 1602 served entropy collapse, where a
 1603 disproportionate number of atten-
 1604 tion heads exhibited extremely low
 1605 entropy values, ranging from 0 to $\frac{\text{Max}}{4}$, with most values near zero.
 1606



1607 Figure 16: Head-wise entropy distribution in the Softmax-only
 1608 GPT-2 model ($L=12$, $H=12$, $d=768$) with earlier FFNs intact
 1609 and deeper FFNs pruned, trained from scratch on the CodePar-
 1610 rot dataset.

1611 To investigate this instability further, Figure 17 provides a detailed analysis. Training stability
 1612 is maintained when up to 6 FFNs are pruned, as shown by the layer-wise entropy dynamics and
 1613 heatmaps, which resembles the behavior of the unpruned SM + ScFuFFN model. In particular, both
 1614 models have approximately 55% to 60% of attention heads exhibiting entropy values in the balanced
 1615 range, with negligible attention heads falling within the 0 to $\frac{\text{Max}}{4}$ range. However, pruning the 7th FFN
 1616 (SM + ScFuFFNi₇) leads to a sudden shift, resulting in NaNs and entropy collapse, particularly in the
 1617 deeper layers. The similarity in entropy dynamics and heatmaps between the stable configurations
 1618 suggests that the model remains robust as long as no more than 6 FFNs are pruned.
 1619

1620 Nonetheless, all the pruned and unpruned models exhibit entropic overload, where a significant
 1621 fraction of attention heads possess high entropy values in the range $\frac{3\text{Max}}{4}$ to Max, stable models
 1622 exhibiting this overload to a lesser extent.

1623 D.8 MITIGATING OVER-REGULARIZATION WITH AN APPROPRIATE THRESHOLD MARGIN
 1624

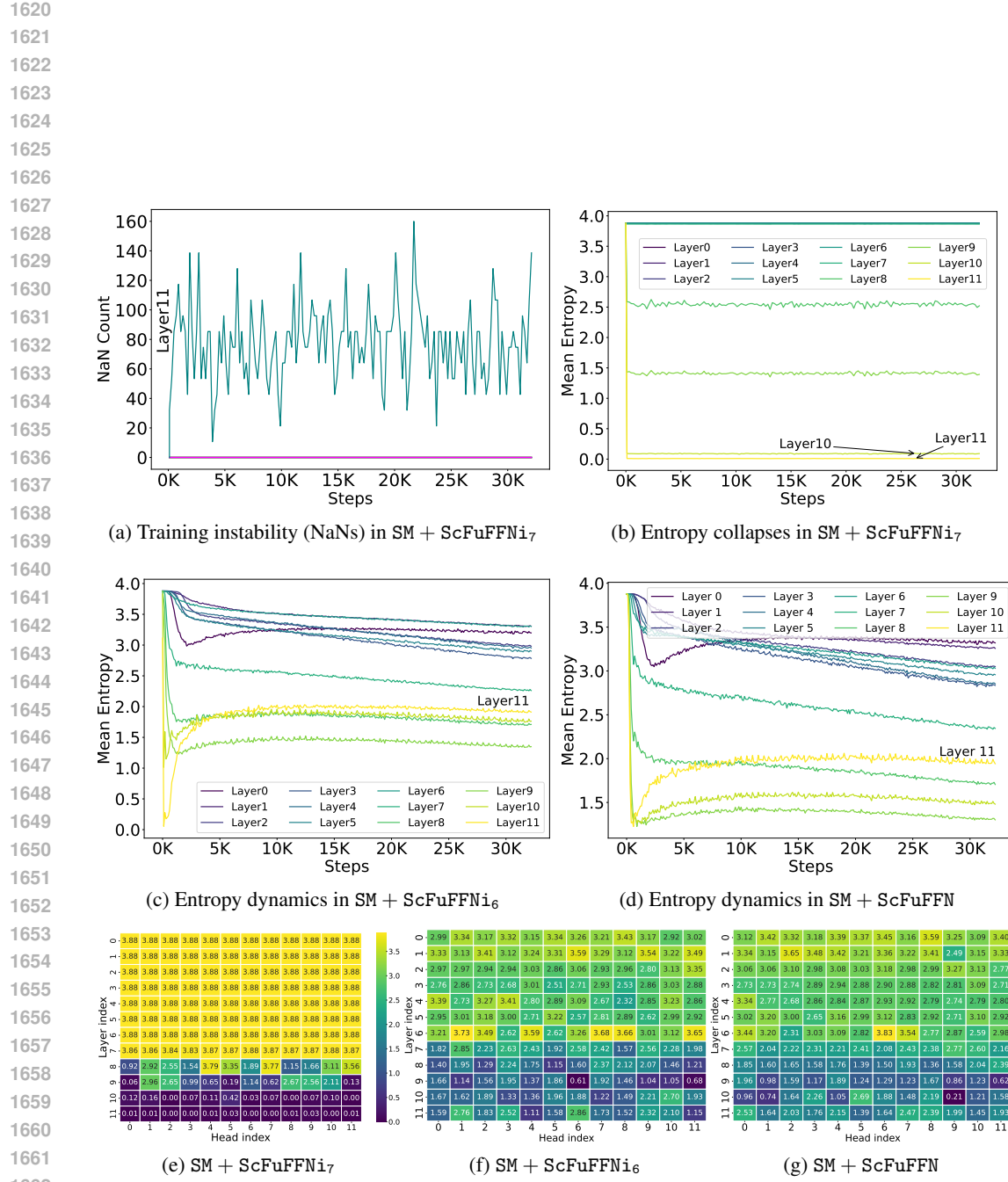


Figure 17: Training instability is evident with NaNs in the final layers (a) and entropy collapse in the last two layers (b) of the SM + ScFuFFNi₇ configuration, where 7 deeper FFNs are pruned in the Softmax-only GPT-2 model ($L = 12, H = 12, d = 768$), trained from scratch on the CodeParrot dataset. In contrast, stable training is observed in (c) with no entropy collapse when only 6 deeper FFNs are pruned (SM + ScFuFFNi₆), and further validated against the unpruned configuration (SM + ScFuFFN) in (d). The last row (e, f, g) shows entropy heatmaps for each configuration.

Figure 18 illustrates the effect of γ on the headwise entropy distribution. The hyperparameter γ employed to adjust the threshold margin in entropy regularization, defined as $Tol_{\text{margin}} = \gamma E_{\max}$ (Algorithm1, line #3), effectively preventing over-regularization by ensuring that a sufficient fraction of heads maintains entropy values in the upper range $\frac{3\text{Max}}{4}$ to Max. As γ increases from 0 to 0.15, only a small proportion of attention heads (0.7%) are situated in the highest entropy range. However, as γ is increased beyond 0.15, the fraction of heads in this upper range starts increasing, reaching 2.08%, 3.47%, and 6.25% at $\gamma=0.20, 0.25$, and 0.30 , respectively.

This fine-grained control on the population of attention heads in the higher entropy range highlights the ability of entropy regularization to prevent over-regularization and maintain the attention heads' diversity. We find that $\gamma=0.2$ yields slightly better performance in terms of lower perplexity compared to higher γ values, and thus, we adopt this value in the final entropy regularization scheme.

To better understand the increase in the fraction of attention heads with higher γ , Figure 19 illustrates the layerwise entropy dynamics during training. Notably, at higher γ , the fraction of attention heads with higher entropy values increases, as indicated by the increases in the mean entropy of the early layers, which helps to prevent over-regularization and maintain heads' diversity.

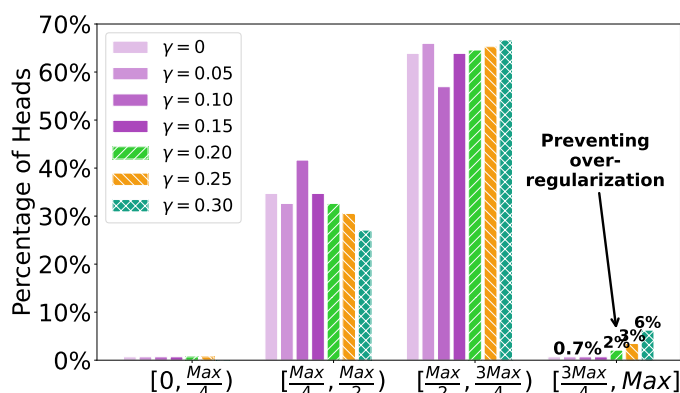
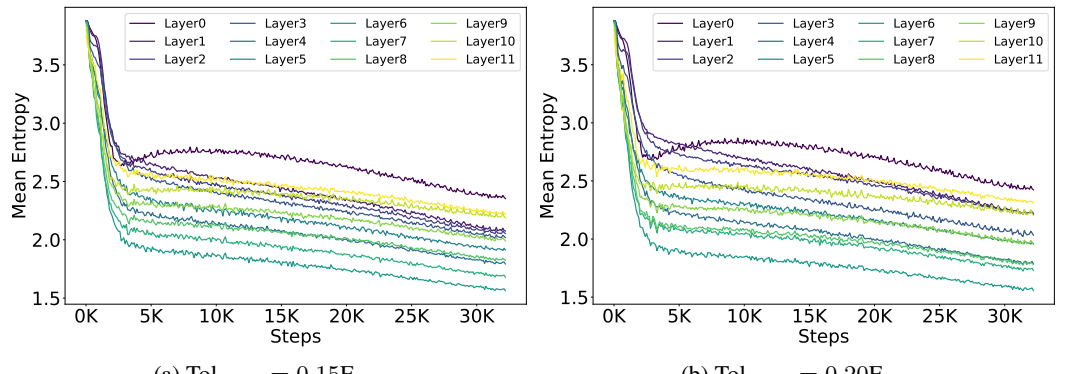
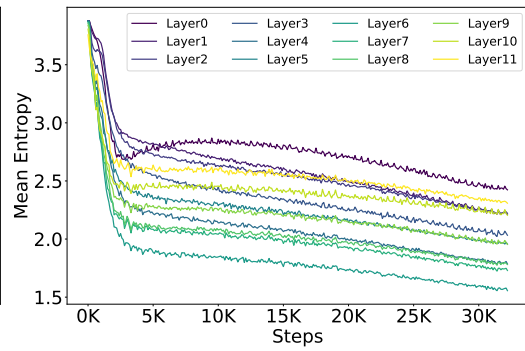


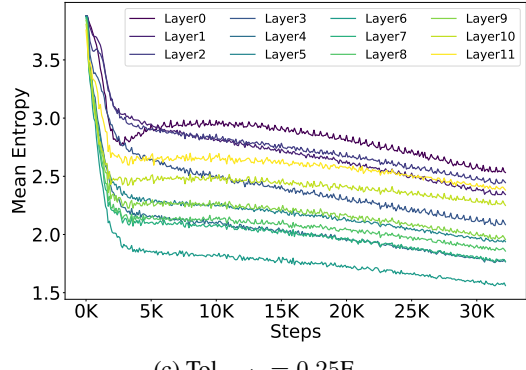
Figure 18: Headwise entropy distribution in the SM(t) + ScFuFFN GPT-2 model ($L=12$, $H=12$, $d=768$) when entropy regularization is applied with varying threshold margin, controlled by hyperparameter γ .



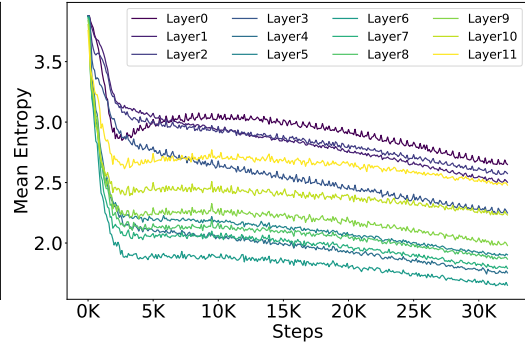
(a) $\text{Tol}_{\text{margin}} = 0.15E_{\max}$



(b) $\text{Tol}_{\text{margin}} = 0.20E_{\max}$



(c) $\text{Tol}_{\text{margin}} = 0.25E_{\max}$



(d) $\text{Tol}_{\text{margin}} = 0.30E_{\max}$

Figure 19: Layerwise entropy dynamics when entropy regularization is employed with increasing threshold margin, defined as $\text{Tol}_{\text{margin}} = \gamma E_{\max}$ (see Algorithm1, line #3). At higher γ , the mean entropy of the early layers increases.

1728 **E FLOPs COMPUTATION FOR INFERENCE**
 1729

1730 To generate one output token during inference, the model performs a forward pass over a sequence of
 1731 length L (the context size). Below, we detail the FLOPs required for both the feed-forward (FFN)
 1732 and self-attention sub-blocks. We compute the *FLOPs per token per layer* as follows:

- 1733 • **FFN FLOPs:** The FFN sub-block consists of two linear transformations, parameterized by
 1734 $\mathbf{W}_{\text{in}}^{\text{ffn}} \in \mathbb{R}^{d \times 4d}$ and $\mathbf{W}_{\text{out}}^{\text{ffn}} \in \mathbb{R}^{4d \times d}$. Each layer contributes equally to the FLOPs count. The total
 1735 FLOPs for the FFN can be expressed as:

$$1736 \text{FFN FLOPs} = 2 \times 2 \times (d \times 4d) = 16d^2$$

1737 - The first factor of 2 accounts for the two linear layers, while the second factor of 2 arises because
 1738 each dot product in a matrix-matrix multiplication involves two floating point operations—one
 1739 multiplication and one addition (Performance, 2023).

- 1740 • **Self-Attention FLOPs:** The breakdown for attention FLOPs is presented as follows:

- 1741 1. **Linear projections (\mathbf{W}^Q , \mathbf{W}^K , \mathbf{W}^V , and \mathbf{W}^O) FLOPs:** The input sequence of shape $\mathbb{R}^{T \times d}$
 1742 is linearly transformed using weights of shape $\mathbb{R}^{d \times d}$ across four linear layers (for queries,
 1743 keys, values, and output projection). Thus, the total FLOPs for these operations are:

$$1744 4 \times 2 \times T \times (d \times d) = 8Td^2$$

1745 Since we are interested in FLOPs per token, this simplifies to $8d^2$

- 1746 2. **Attention Matrix ($\mathbf{Q}\mathbf{K}^T$) Computation:** The attention mechanism involves computing
 1747 the dot product between the query matrix $\mathbf{Q} \in \mathbb{R}^{T \times d_k}$ and the transposed key matrix
 1748 $\mathbf{K}^T \in \mathbb{R}^{d_k \times T}$. For each attention head, this operation results in:

$$1749 2 \times T \times d_k \times T$$

1750 With H heads, the total FLOPs for this step are:

$$1751 2 \times H \times (T \times d_k \times T) = 2dT^2$$

1752 Hence, FLOPs per token simplifies to $2dT$.

- 1753 3. **Dot Product with \mathbf{V} :** After calculating the attention weights, the values matrix $\mathbf{V} \in \mathbb{R}^{T \times d_k}$
 1754 is multiplied by the attention scores. Due to the masking in the upper triangular attention
 1755 matrix (to enforce causality), only the lower triangular part of the matrix is involved in the
 1756 computation. The number of FLOPs per head is:

$$1757 2 \times d_k \times \frac{T(T+1)}{2}$$

1758 For H heads, this totals to:

$$1759 2 \times d \times \frac{T(T+1)}{2}$$

1760 Thus, the FLOPs per token for this step are:

$$1761 d \times (T+1)$$

1762 Combining all components, the total FLOPs for self-attention per token is:

$$1763 \text{Self-attention FLOPs} = 8d^2 + 2Td + d(T+1)$$

1764 In summary, the FLOPs computation for one layer includes both the FFN and self-attention sub-blocks,
 1765 yielding the following total per token:

$$1766 \text{Total FLOPs per token per layer} = \underbrace{16d^2}_{\text{FFN}} + \underbrace{(8d^2 + 3Td + d)}_{\text{Self-attention}}$$

1767 Total FLOPs with L layers and T tokens (context length) = $L \times T \times (24d^2 + 3Td + d)$

1768 Note that the FFN FLOPs depend on the hidden dimension, a design hyperparameter typically set as a
 1769 multiple of the model dimension d , which varies across LLM architectures, for example, $4d$ in GPT-2

(Radford et al., 2019; Brown et al., 2020) and Pythia(Biderman et al., 2023), $\frac{8d}{3}$ in LLaMA(Touvron et al., 2023), $3.5d$ in Mistral Jiang et al. (2023), and $8d$ in Gemma Team et al. (2024).

Now, we want to analyze which component, FFN or self-attention, dominates the total FLOPs count of a given architecture. For this, we solve the following inequality:

$$\begin{aligned} 1787 \quad 16d^2 &> 8d^2 + 3dT + d \implies 8d^2 > d(3T + 1) \implies 8d - 1 > 3T \implies T < \frac{8d - 1}{3} \\ 1788 \quad &\implies T < \frac{8d}{3} \quad (\text{To simplify, we approximate } 8d - 1 \approx 8d) \end{aligned} \quad (13)$$

It is evident that in the shorter context length regime, where $T < \frac{8d}{3}$, the FFN FLOPs dominate the total FLOPs. Thus, for tasks with smaller context lengths, optimizing the FFN sub-block can lead to efficiency gains, while for larger contexts, self-attention FLOPs become more significant. Therefore, understanding this FLOPs distribution can guide efficient architectural design for private inference, depending on the expected context size.

E.1 DISTRIBUTION OF FLOPS IN GPT-2 MODELS

Figure 20 illustrates the distribution of FLOPs between the attention and FFN sub-blocks across different context sizes for GPT-2 models, ranging from 128 to 8K tokens.

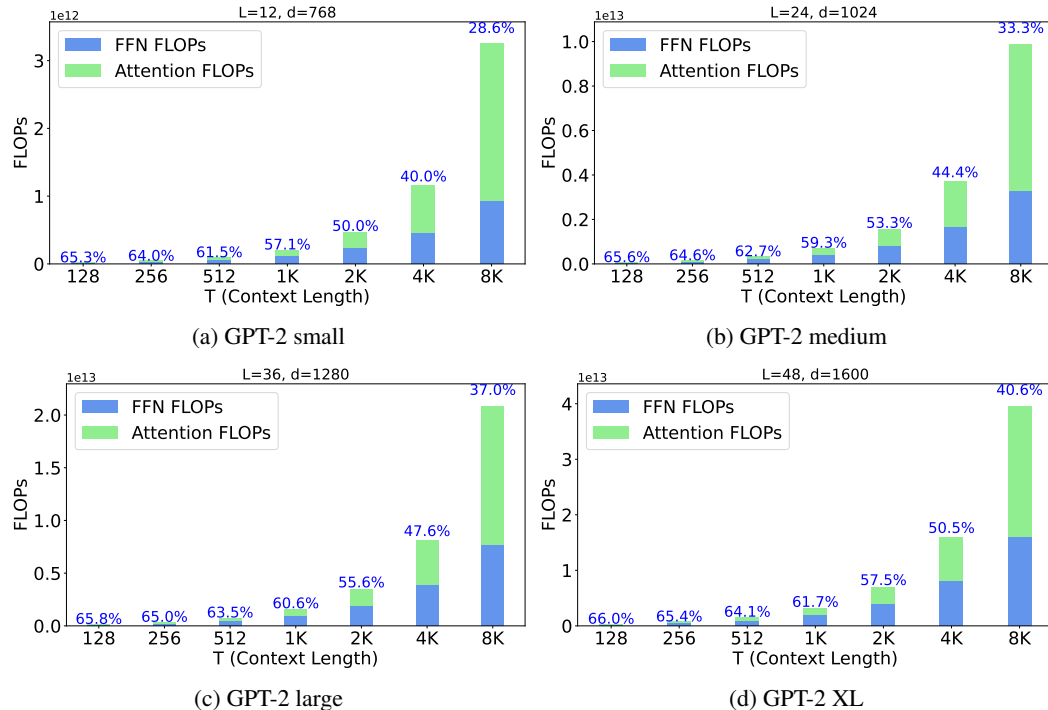


Figure 20: FLOPs breakdown in GPT-2 models for a single forward pass: Up to a context length of 2K, FFN operations are the primary contributors to FLOPs. Beyond 8K, attention operations start to dominate (Percentage on top of each bar represents the proportion of FFN FLOPs)

E.2 DISTRIBUTION OF FLOPS IN PYTHIA MODELS

Figure 21 illustrates the distribution of FLOPs between the attention and FFN sub-blocks across different context sizes for Pythia models, ranging from 128 to 8K tokens.

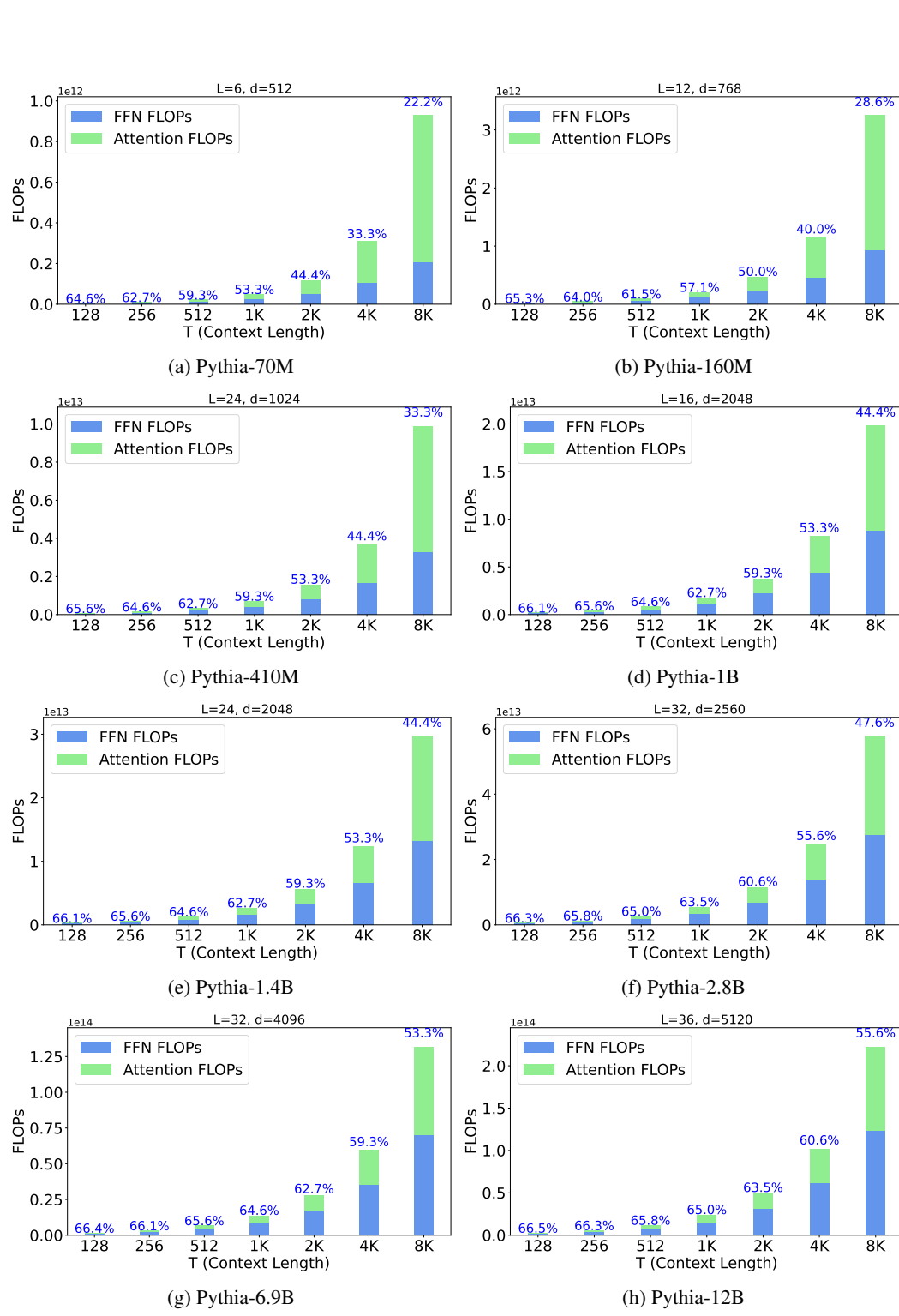


Figure 21: FLOPs breakdown in Pythia models for a single forward pass: Similar to GPT-2 models (see Figure 20), FLOPs are dominated by FFN operations up to a context length of 4K, except for smaller models where FFN operations dominate up to 2K (Percentage on top of each bar represents the proportion of FFN FLOPs).

1890 F ADDITIONAL RELATED WORK 1891

1892 **The Pitfalls of LayerNorm in LLM** While LayerNorm is a critical source of non-linearity in both
1893 CNNs (Ni et al., 2024) and transformer-based models (Wu et al., 2024; Zhao et al., 2024; Joudaki
1894 et al., 2023), it causes several challenges in the transformer-based LLMs that extend well-beyond PI.
1895

1896 First, in PI with hybrid protocols, the inverse-square root computation poses significant challenges
1897 for its precise computation. Also, in HE-only PI, the polynomial approximation of LayerNorm is
1898 quite challenging because of the unusually wide range of its variance values Zimerman et al. (2024).
1899

1900 Furthermore, the trainable parameters in LayerNorm are shown to be associated with the outlier
1901 features in LLMs He et al. (2024); Bondarenko et al. (2023); Wei et al. (2022); Kovaleva et al. (2021),
1902 posing significant issues in LLM quantization. Specifically, the scaling parameters in LayerNorm
1903 amplify outlier features, which in turn makes low-precision training challenging Wei et al. (2022).
1904

1905 Moreover, LayerNorm introduces difficulties in mechanistic interpretability, as it tends to make the
1906 residual stream more complex and harder to analyze Nanda (2023).
1907

1908 Also, from the perspective of signal propagation theories, LayerNorm negatively impacts the train-
1909 ability of LLMs He & Hofmann (2024); He et al. (2023).
1910

1911 **Entropy Regularization** Entropy regularization has been widely applied in various areas of machine
1912 learning. It has been used to penalize low entropy predictions (Pereyra et al., 2017) and to maximize
1913 predictions’ entropy (Setlur et al., 2022). It has also been used to improve adversarial robustness
1914 (Jagatap et al., 2022), to avoid bad initializations and local minima (Miller et al., 1996), to optimize
1915 the layer-wise flow of information in deeper networks (Peer et al., 2022), to balance exploration-
1916 exploitation and promote action diversity in reinforcement learning (Wang et al., 2024; Ahmed et al.,
1917 2019; Lu & Van Roy, 2019; Neu et al., 2017; Mnih, 2016), and for domain generalization (Zhao
1918 et al., 2020).
1919

1920 **The Role of Nonlinearity in LLM** Understanding the role of nonlinearity in the transformer-based
1921 models is an emerging research area. Li et al. (2024) offer a theoretical analysis on the role of attention
1922 and FFN nonlinearity for in-context learning tasks. However, their work is limited to a simplified,
1923 one-layer model consisting of a single softmax-based self-attention head and a ReLU-based FFN.
1924 Nonetheless, Cheng et al. (2024) explore a broader range of nonlinear architectures and in-context
1925 learning tasks, demonstrating that the optimal activation function can vary depending on the specific
1926 function class the model is attempting to learn.
1927

1928 G DISCUSSION 1929

1930 G.1 LINEAR VS. NON-LINEAR FFNS: PRIVILEGED BASIS AND ROTATIONAL INVARIANCE 1931

1932 In transformer-based architectures, there is a crucial distinction between linear and non-linear
1933 transformations, particularly when analyzing the *privileged basis* phenomenon (Elhage et al., 2023).
1934

1935 A *privileged basis* occurs when certain directions in the network’s activation space are favored due
1936 to the network’s architecture. Specifically, non-linear activations (e.g., ReLU, GELU) encourage
1937 features to align with specific directions in the hidden space, breaking the rotational invariance of the
1938 network. This alignment forces neurons to prioritize specific directions or features, leading to a basis
1939 that is more interpretable but inherently dependent on the chosen non-linear function.
1940

1941 **Non-linear FFN** In a conventional FFN, the architecture includes two linear transformations with a
1942 non-linear activation between them. This non-linearity breaks the rotational invariance of the hidden
1943 space, as the activation function behaves differently depending on the input direction. Mathematically,
1944 this can be described as:
1945

$$1946 \text{FFN}_{\text{non-linear}}(x) = \sigma(x\mathbf{W}_{\text{in}}^{\text{ffn}} + \mathbf{b}_1)\mathbf{W}_{\text{out}}^{\text{ffn}} + \mathbf{b}_2$$

1947 Where $\sigma(\cdot)$ represents the elementwise non-linearity, which restricts the model from treating all
1948 directions in the hidden space equally, thereby establishing a *privileged basis*.
1949

1944
 1945 **Linear FFN** Removing the non-linearity from the FFN results in a purely *linear transformation*,
 1946 which preserves rotational invariance in the hidden space. The linear FFN operates as:
 1947
 1948

$$\text{FFN}_{\text{linear}}(x) = (x \mathbf{W}_{\text{in}}^{\text{ffn}}) \mathbf{W}_{\text{out}}^{\text{ffn}} + \mathbf{b}$$

1949 Without the activation function, the representations remain invariant under rotations, meaning that no
 1950 specific direction is favored over others. In a *linear FFN*, the model retains its flexibility in how it
 1951 represents features, without forcing any particular alignment of neurons. In effect, the model operates
 1952 in a *non-privileged basis*, allowing the representation to rotate freely in the vector space.
 1953

G.2 EARLY VS. DEEPER FFNS

1954 Early FFNs in transformer models are particularly critical due to the presence of polysematic
 1955 neurons(Ferrando et al., 2024), which can respond to multiple, unrelated features simultaneously.
 1956 These neurons enable early layers to detect broad and diverse patterns, such as linguistic structures,
 1957 n-grams, and other foundational features of the input. This general-purpose functionality allows the
 1958 early FFNs to play a vital role in the initial stages of context formation, capturing a wide range of
 1959 information necessary for effective processing in later stages.
 1960

1961 Additionally, research highlights that early layers play a pivotal role in the memorization and recall
 1962 of factual information (Haviv et al., 2023; Meng et al., 2022). These layers not only capture general
 1963 patterns but also store and retrieve memorized knowledge, promoting the predicted token to the
 1964 top of the output distribution. This suggests that early FFNs are integral for accessing learned
 1965 information, making them crucial for both context formation and recalling facts essential to the
 1966 model’s predictions.
 1967

1968 In contrast, deeper FFNs become more specialized, focusing on refining the information extracted by
 1969 the earlier layers. They process the data with a narrower scope, tailoring it for task-specific outputs.
 1970 While these deeper layers are essential for fine-tuning the model’s predictions, the early FFNs are key
 1971 to generalizing over complex and varied input patterns, establishing the groundwork for the model’s
 1972 overall performance.
 1973

H FUTURE WORK

1974 To further reduce non-linear operations in our Softmax-only architecture, off-the-shelf head pruning
 1975 techniques Voita et al. (2019); Michel et al. (2019); Jo & Myaeng (2020); Ma et al. (2021); Li et al.
 1976 (2022) can be applied on top of AERO. Another approach is to explore linear softmax operations.
 1977 However, these linear softmax operations sometimes introduce additional normalization layers or
 1978 complex activation functions in the FFN Zhang et al. (2024), which could increase the PI overheads,
 1979 counteracting the intended efficiency improvements.
 1980

1981 Additionally, incorporating weight and activation quantization Wu et al. (2023); Xiao et al. (2023);
 1982 Dettmers & Zettlemoyer (2023) could further enhance the efficiency of private inference in our
 1983 architecture.
 1984

1985 Orthogonally, performance improvement techniques such as knowledge distillation (KD) can be
 1986 employed to complement these optimizations Ko et al. (2024); Liang et al. (2023); Gu et al. (2023);
 1987 Hsieh et al. (2023); Li et al. (2023b).
 1988

1989 Looking ahead, scaling AERO to more complex and deeper LLMs can be achieved by strategically
 1990 combining techniques such as weight normalization, spectral normalization, and FFN output scaling.
 1991 These methods can be applied selectively, with different layers using different techniques—for
 1992 instance, employing spectral normalization in early layers and FFN output scaling in deeper layers.
 1993 This tailored approach could lead to better stability and efficiency in larger models.
 1994

I AERO BEYOND PRIVATE INFERENCE: BROADER IMPACT AND PROMISES

1995 While AERO originally developed to enable efficient private inference in transformer-based lan-
 1996 guage models by reducing cryptographic overheads, its architectural innovations and insights have
 1997

1998 far-reaching implications beyond privacy-preserving computations. Its principled approach for architectural simplifications and techniques for maintaining model stability offer valuable insights into the broader field of language model design and optimization.

1999

2000

2001 Here, we explore how AERO’s principles can influence various facets of standard transformer architectures and their applications. These broader implications span from fundamental architectural design choices to practical deployment considerations, demonstrating how techniques developed for private inference can enhance the understanding and implementation of LLMs.

2002

2003

2004

2005

2006 **Plaintext efficiency** Our finding that ReLU naturally emerges as the preferred activation function in LayerNorm-free architectures aligns well with plaintext efficiency goals. ReLU’s ability to induce sparsity in activations accelerates the plaintext inference by reducing the data traffic between CPU and GPU Mirzadeh et al. (2024).

2007

2008

2009

2010 Furthermore, AERO introduces a systematic approach for reducing FLOPs by designing *linear FFNs*, which enable the fusion of linear layers into a single transformation and reduces FFN FLOPs by $8\times$.

2011

2012 Moreover, AERO replaces deeper FFNs with identity connections without compromising training stability, resulting in *additional* FLOPs reductions. These optimizations are particularly effective for inference with smaller context lengths ($T < \frac{8d}{3}$), where FFN FLOPs dominates.

2013

2014

2015 **Low-precision training and quantization for resource-constrained applications** The deployment of transformer models in resource-constrained environments is significantly hindered by outliers that complicate low-bitwidth quantization. These outliers emerge from two primary sources: softmax-based attention mechanism Hu et al. (2024b) and LayerNorm layers He et al. (2024); Wei et al. (2022); Kovaleva et al. (2021). LayerNorm-induced outliers are particularly *severe* as their scaling parameters amplify activation extremes, demanding higher bit-widths for accurate representation.

2016

2017

2018

2019

2020

2021 Our LayerNorm-free design inherently addresses the major source of outliers by completely removing the problematic scaling parameters. While empirical validation remains necessary, the LayerNorm-free architectural choices in the AERO framework point to promising directions for enabling low-precision training and quantization, where effective outlier management is critical.

2022

2023

2024

2025 **An information-theoretic approach for understanding the role of nonlinearity in LLMs** While prior work has examined the role of nonlinearities in in-context learning (Cheng et al., 2024; Li et al., 2024), AERO introduces an information-theoretic perspective to analyze their impact in LLMs. By employing Shannon’s entropy as a quantitative measure, we characterize how architectural choices influence attention score distributions in MHA sub-block.

2026

2027

2028

2029

2030 Our analysis reveals that nonlinearities in LLMs serve a *dual purpose*: they are essential not only for training stability but also for preserving attention head diversity, enabling the optimal utilization of MHA’s representational capacity. Consequently, their removal can destabilize training, leading to entropy collapse in deeper layers, or result in the underutilization of MHA’s representational capacity, as evidenced by entropic overload in early layers—or both.

2031

2032

2033

2034

2035 **Insights into mechanistic interpretability and disentangling polysemantic neurons** By stripping away complex nonlinearities, such as GELU and LayerNorm, AERO makes it easier to dissect how individual neurons, attention mechanisms, and linear FFNs contribute to model behavior, thereby facilitating a more *granular* understanding of the internal dynamics of LLMs.

2036

2037

2038

2039 In standard transformer architectures, nonlinearities like GELU induce complex feature interactions, often resulting in polysemantic neurons—neurons that encode overlapping or unrelated information Gurnee et al. (2023); Mu & Andreas (2020). By simplifying the FFN to a purely linear structure, AERO could minimize feature entanglement, fosters monosemantic neuron behavior, and produces a more disentangled and interpretable neuron space Pearce et al. (2024)

2040

2041

2042

2043

2044

2045

2046

2047

2048

2049

2050 Moreover, while not explicitly explored in Gould et al. (2024); Kissane et al. (2024), there may be intriguing connections between the entropy regularization in AERO, which dynamically adjusts to head-specific behavior, and the insights offered by attention heads that inherently encode interpretable patterns. This suggests the possibility that entropy-guided, adaptive attention mechanisms could facilitate the emergence or identification of such interpretable structures.

2051 **Parallels between entropy-guided attention and differential attention mechanism** In principle, our entropy regularization scheme shares fundamental similarities with the recently proposed Differential Transformer architecture Ye et al. (2024), despite their distinct implementations.

2052 Just as the differential attention mechanism nullifies attention noise through contrastive learning, our
 2053 entropy-guided attention mechanism can be tailored to achieves similar effects by penalizing attention
 2054 dispersal across tokens. Both approaches effectively promote *sparse* attention patterns: Differential
 2055 Transformer achieves this through computing differences between attention maps, while our entropy
 2056 regularization specifically penalizes high-entropy attention distributions.

2057 These connections demonstrate that promoting selective attention can be achieved either through
 2058 architectural design or through careful entropy regularization, offering complementary approaches to
 2059 the same underlying objective.

2060 **Entropy-guided solution for attention sink and attention noise** The softmax operation in
 2061 transformer-based attention mechanisms inherently assigns non-zero probabilities to all tokens
 2062 due to its normalized exponential form. This leads to two key issues: disproportionate emphasis on
 2063 specific tokens (attention sink) Xiao et al. (2024); Cancedda (2024); Gu et al. (2024); and non-zero
 2064 scores for irrelevant tokens (attention noise), which may leads to hallucinations Ye et al. (2024),
 2065 outlier activations Hu et al. (2024b), and inefficient use of model capacity.

2066 While recent works Yin et al. (2024); Yu et al. (2024) have proposed various solutions, AERO intro-
 2067 duces a principled approach with its adaptive entropy regularization to control attention distribution.
 2068 By penalizing excessively high entropy values and incorporating learnable threshold parameters,
 2069 AERO enables each attention head to adaptively determine its optimal degree of focus. This could
 2070 prevent the over-diffusion of attention scores while *preserving* the mathematical properties of softmax.

2071

2072 **New scientific opportunities for understanding training instability** Recently, there has been
 2073 significant interest in understanding training instability in transformer models Wortsman et al. (2024);
 2074 Rybakov et al. (2024); Zhai et al. (2023). While these studies provide valuable insights, they predom-
 2075 inantly focus on standard transformer architecture, leaving a critical question unaddressed: *How do
 2076 architectural simplifications, such as the removal of non-linearities, impact training dynamics?*

2077 Our work provides the first comprehensive investigation of how the systematic removal of nonlin-
 2078 earities impacts training stability, specifically through the lens of entropy dynamics, offering novel
 2079 insights for understanding the interplay between model design and training dynamics.

2080 Prior research has focused on instability factors such as the unbounded growth of attention logits
 2081 Zhai et al. (2023); Dehghani et al. (2023). In contrast, our entropy-based analysis reveals a previously
 2082 unexplored contributor to training stability: *linear FFNs*. Notably, we demonstrate that linear FFNs,
 2083 especially in the early layers, are critical for preventing entropy collapse during training.

2084 While our experiments use smaller models like GPT-2, the findings on training instability extend to
 2085 larger models, as prior research Wortsman et al. (2024) shows similar patterns persist at scale.

2086

2087 **Static alternatives for training stability solutions** To address training instability, prior work
 2088 has predominantly relied on LayerNorm applied to various parts of the network, such as QK-
 2089 LayerNorm Dehghani et al. (2023); Wortsman et al. (2024); Rybakov et al. (2024). In contrast,
 2090 our approach demonstrates the effectiveness of static alternatives like weight normalization and
 2091 spectral normalization. These methods mitigate entropy collapse in deeper layers while avoiding the
 2092 computational overhead and non-linear operations associated with LayerNorm during inference.

2093 **Entropy-guided solutions for uncertainty estimation and mathematical reasoning** Recent ad-
 2094 vancements, such as the entropy-guided sampling method (e.g., the Entropix framework Team (2024))
 2095 and the discovery of entropy neurons which regulate uncertainty in next-token predictions Gurnee
 2096 et al. (2024); Stolfo et al. (2024), highlight a significant shift toward entropy-guided LLMs solutions.

2097 These approaches have the potential to address token-level challenges in mathematical reasoning
 2098 tasks Langlais (2024). The recently introduced FrontierMath benchmarks Glazer et al. (2024), which
 2099 have garnered significant attention from the research community, further emphasize the importance
 2100 of improving the mathematical reasoning capabilities in LLMs.

2101 The key insight from this line of research is that different mathematical operations may require
 2102 varying levels of token selection certainty. For instance, basic arithmetic operations might benefit
 2103 from more deterministic (low-entropy) token selection, whereas complex problem-solving tasks could
 2104 thrive on more exploratory (high-entropy) patterns.

2105

2106 While AERO’s current entropy regularization focuses on attention patterns, it could be adapted beyond
2107 attention patterns to also guide token selection during inference, similar to the *adaptive temperature*
2108 strategies that adjust model creativity based on logit entropy Veličković et al. (2024). Another
2109 potential approach would be to introduce controlled entropy pathways specifically for numerical
2110 operations, and different entropy thresholds for different types of mathematical tasks.

2111 Furthermore, AERO’s architecture could be augmented with specialized *reasoning tokens*, inspired
2112 by pause tokens designed for reasoning steps Langlais (2024). By extending entropy regularization
2113 to guide the model’s behavior around these reasoning tokens, we could enable more structured and
2114 interpretable mathematical reasoning paths.
2115
2116
2117
2118
2119
2120
2121
2122
2123
2124
2125
2126
2127
2128
2129
2130
2131
2132
2133
2134
2135
2136
2137
2138
2139
2140
2141
2142
2143
2144
2145
2146
2147
2148
2149
2150
2151
2152
2153
2154
2155
2156
2157
2158
2159